The genetic and dietary landscape of the muscle insulin signalling network

Julian van Gerwen[1], Stewart W. C. Masson[1], Harry B. Cutler[1], Alexis Díaz-Vegas[1], Meg Potter[1], Jacqueline Stöckli[1], Søren Madsen[1], Marin E. Nelson[1], Sean J. Humphrey[1], David E. James[1,2,3]

1. Charles Perkins Centre, School of Life and Environmental Sciences, University of Sydney, 2006, Australia

2. Faculty of Medicine and Health, University of Sydney, 2006, Australia

3. Lead contact

Correspondence:

david.james@sydney.edu.au

sean.humphrey@mcri.edu.au

Abstract

Metabolic disease is caused by a combination of genetic and environmental factors, yet few studies have examined how these factors influence signal transduction, a key mediator of metabolism. Using mass spectrometry-based phosphoproteomics, we quantified 23,126 phosphosites in skeletal muscle of five genetically distinct mouse strains in two dietary environments, with and without acute *in vivo* insulin stimulation. Almost half of the insulin-regulated phosphoproteome was modified by genetic background on an ordinary diet, and high-fat high-sugar feeding affected insulin signalling in a strain-dependent manner. Our data revealed coregulated subnetworks within the insulin signalling pathway, expanding our understanding of the pathway's organisation. Furthermore, associating diverse signalling responses with insulin-stimulated glucose uptake uncovered regulators of muscle insulin responsiveness, including the regulatory phosphosite S469 on Pfkfb2, a key activator of glycolysis. Finally, we confirmed the role of glycolysis in modulating insulin action in insulin resistance. Our results underscore the significance of genetics in shaping global signalling responses and their adaptability to environmental changes, emphasizing the utility of studying biological diversity with phosphoproteomics to discover key regulatory mechanisms of complex traits.

Introduction

Protein post-translational modifications such as phosphorylation enable cells to rapidly respond to environmental changes by modifying protein function at low metabolic cost[1]. As a result of this high metabolic efficiency, phosphorylation is involved in nearly all biological processes and is dysregulated in numerous complex diseases[2]. Advances in mass spectrometry-based phosphoproteomics – the unbiased identification and quantification of protein phosphorylation – have led to the discovery of more than 100,000 phosphosites, revealing that the phosphoproteome comprises vast, interconnected phosphorylation networks[3–6], rather than the textbook view of isolated, linear kinase cascades.

The insulin signalling network is among the most studied phosphorylation networks. Post-prandial increases in blood glucose stimulate pancreatic insulin secretion, coordinating a metabolic switch in target tissues like skeletal muscle and adipose[7]. Insulin increases glucose uptake into these tissues by promoting translocation of the glucose transporter GLUT4 to the plasma membrane, and serves other functions like enhancing protein synthesis, downregulating lipid catabolism, and altering gene transcription[7]. To coordinate these functions, insulin triggers a phosphorylation cascade primarily involving activation of the Ser/Thr kinase Akt, regulation of downstream kinases including mTORC1 and GSK3, and modulation of parallel signalling arms[7–9]. Seminal phosphoproteomics studies demonstrated that this cascade regulates over a thousand phosphosites, with many still uncharacterised in insulin action[10–12]. Insulin resistance – the failure of insulin to promote glucose uptake in its target tissues – is triggered by genetic and environmental factors such as family history of metabolic disease and high-calorie diets[13]. Although insulin resistance is a major precursor of metabolic disease including type 2 diabetes, its mechanistic basis remains unresolved[13–15].

Interactions between genetics and environment significantly regulate biomolecular processes, including insulin resistance[16–19]. As signalling pathways connect the extracellular environment to intracellular proteins, they are likely a major conduit of gene-by-environment interactions. Yet, how global phosphorylation signalling networks are regulated across different genetic backgrounds is relatively unexplored. Recent phosphoproteomics studies in yeast[20] and mice[21] identified genetic variants affecting multiple phosphosites, but did not analyse the phosphoproteome's response to acute perturbation, which is crucial to its role as a signal transduction system. We have also shown marked variation in acute signalling responses to exercise or insulin across individuals[22]. However, this study did not systematically assess the relative contributions of genetics and the environment[22]. Understanding how these variables intersect with signal transduction is fundamental to our basic knowledge of signalling and the advancement of personalised medicine, which advocates individualised treatment regimens based on genetic risk factors and gene-by-environment interactions[16,23].

Inbred mice allow precise control of genetics and environment unachievable in human studies, enabling examination of how these factors interact to influence biomolecular systems[24]. Here, we performed phosphoproteomics on insulin-stimulated or control skeletal muscle from five genetically distinct inbred mouse strains fed either an ordinary chow diet or a high-fat, high-sugar "western style"

diet. Strikingly, we found that genetic background influenced both the phosphoproteomic insulin response of chow-fed mice, as well as how these responses were modified by high-fat, high-sugar feeding. These signalling changes were reflected in altered activity profiles of multiple kinases and provided insight into the functional organisation of the insulin signalling network by revealing subnetworks of coregulated phosphosites. A major challenge in phosphoproteomics studies is pinpointing important regulatory events among the many responding to a stimulus. We reasoned that associating changes in protein phosphorylation across the gene-by-environment landscape with phenotypic change – in this case insulin-stimulated glucose uptake – would dissect mechanistic targets with greater fidelity. This approach generated known as well as candidate regulators of insulin-stimulated glucose uptake, leading us to demonstrate that glycolytic upregulation reverses insulin resistance. Our work represents the first global portrait of insulin signalling network plasticity in response to genetic and environmental variation, which will serve as an important resource in future studies of insulin action and resistance.

Results

Phosphoproteomics of insulin signalling in mouse skeletal muscle

To study how protein phosphorylation networks are affected by genetics and environment, we examined insulin signalling in five genetically distinct inbred mouse strains including four lab strains with diverse metabolic phenotypes (C57Bl6J, NOD, BXH9, and BXD34[18]), and the wild-derived CAST strain (**Fig. 1a**). Mice underwent a six-week diet regimen of standard lab diet (CHOW) or a high-fat high-sucrose diet (HFD), which is commonly used to induce insulin resistance[18,25]. Consistent with their diverse genetics, these strains differed in morphometric parameters (body weight, adiposity, lean mas) and metabolic traits (fasting blood glucose, fasting blood insulin, glucose tolerance) both on the CHOW diet and in their response to HFD-feeding (**Fig. S1**).

We focused on skeletal muscle, as it is the site of greatest post-prandial glucose uptake and the most significant contributor to impaired glucose disposal in type 2 diabetes[26]. Specifically, we chose to examine the soleus muscle, because its largely oxidative fibre composition resembles human muscle tissue more than other murine muscles[27]. Mice were injected retro-orbitally with saline control or insulin for 10 minutes, and the soleus was collected for phosphoproteomic analysis (**Fig. 1a**). A tritiated 2-deoxyglucose (^{3}H-2DG) tracer was co-injected to measure soleus glucose uptake.

Using the EasyPhos workflow and data-independent acquisition (DIA) mass spectrometry[28,29], we quantified 28,809 phosphopeptides across 95 biological samples, corresponding to 23,126 unique high-confidence phosphosites (Class I; localization score > 0.75) on 3,507 proteins (**Fig. 1b, Table S1**). On average we quantified 15,395 phosphopeptides in each sample (**Fig. S2a**). Due to the range in soleus mass across strains (**Fig. S1d**) we altered the protein material used for EasyPhos (C57Bl6J and NOD: 755 µg, BXH9 and BXD34: 511 µg, CAST: 364 µg), though phosphopeptide quantification was minimally affected, with only 12.4% fewer phosphopeptides quantified on average in CAST compared

103 to the C57l6J/NOD (average 13891.56 vs 15851.29 **Fig. S2a**). Furthermore, while different strains
104 clustered noticeably by the amount of protein material used, samples from animals of the same strain
105 and diet were still highly correlated and generally clustered together, implying the data are reproducible
106 (**Fig. S2b-d**).

107 To explore the soleus insulin signalling network, we examined phosphopeptides altered by
108 insulin stimulation in at least one of the ten strain-diet combinations. First, to allow comparison across
109 conditions, phosphopeptides were retained if they were quantified well enough to assess the effect of
110 insulin in more than eight strain-diet combinations (≥ 3 insulin-stimulated values and ≥ 3 unstimulated
111 values in each combination). We then tested the resulting 10,432 highly quantified phosphopeptides for
112 significant differences between unstimulated and insulin-stimulated samples (three-way ANOVA
113 insulin main-effect q-value < 0.05) that were of sufficient magnitude in at least one strain-diet
114 combination (insulin/unstimulated fold change > 1.5). This resulted in 441 insulin-regulated
115 phosphopeptides on 232 proteins, which is noticeably more than recent studies of 10-minute insulin
116 signalling in patient-derived myoblasts (174 phosphopeptides[30] and 242 phosphopeptides[31]) or mouse
117 adipose tissue (319 phosphopeptides[32]) (**Fig. 1b, c, Table S1**).

118 Our analysis recovered many well-studied insulin-regulated phosphosites, including Akt
119 substrates such as T247 on Akt1s1 (PRAS40), S939 on Tsc2, and S9 on Gsk3β (**Fig. 1d-f**), as well as
120 targets of downstream kinases including the Gsk3β substrate S641 on Gys1 (**Fig. 1g**). Enrichment of
121 Gene Ontology (GO) biological processes recapitulated canonical insulin signalling axes including
122 "insulin receptor signaling pathway", "phosphatidylinositol 3-kinase signaling", "protein kinase B
123 signaling", and "TORC1 signaling", and multiple pathways related to glucose metabolism, fatty acid
124 metabolism, autophagy, and protein translation, reflecting known targets of insulin action (**Fig. S3a**).
125 Furthermore, insulin-regulated phosphosites were enriched for insulin regulation in our previous human
126 skeletal muscle phosphoproteome (fold enrichment = 4.22, $p = 9.50 \times 10^{-24}$, one-sided Fisher's exact test,
127 **Fig. S3b**)[22]. Despite this, only half of all insulin-regulated phosphopeptides (228/441) were previously
128 annotated as insulin-regulated in the PhosphositePlus database[33] (**Fig. S3c**), highlighting the potential
129 of our data to discover novel aspects of insulin signalling while recapitulating known components. In
130 addition to insulin, exercise also promotes GLUT4 translocation in skeletal muscle[34]. We identified a
131 small subset of phosphosites regulated by insulin in this study that were also regulated by exercise in
132 two separate human phosphoproteomics studies[22,35] (**Fig. S3d, Table S2**, phosphosites: Eef2 T57 and
133 T59, Mff S129 and S131, Larp1 S498, Tbc1d4 S324, Svil S300, Gys1 S645), providing a starting point
134 for exploring conserved signalling regulators of GLUT4 translocation. Overall, our phosphoproteomics
135 data provide a comprehensive and high-quality atlas of insulin signalling in mouse skeletal muscle.
136

137 ***Genetics and diet modulate insulin signalling***

138 The influence of genetic and environmental variation on global insulin signalling responses is largely
139 unknown. We therefore developed a pipeline to address this question using our phosphoproteomics data

140 (**Fig. 2a**). First, we converted the intensity values of each insulin-regulated phosphopeptide to "insulin
141 response" values, by normalising insulin-stimulated data to the unstimulated median of the
142 corresponding Strain-Diet combination. Since protein expression should not change within a 10 min
143 insulin stimulation[32], this allowed us to parse out protein abundance differences across strains and diets
144 and focus solely on acute signalling processes. We then assessed the impact of genetics in CHOW-fed
145 mice by identifying phosphopeptides with differing insulin responses in one or more strains compared
146 to C57Bl6J ("Strain effect"). Lastly, we explored the effects of HFD-feeding on signalling as two types
147 of "Diet effects", either as a "Uniform diet effect" – where HFD-feeding affects each strain similarly –
148 or a "StrainxDiet effect" – where its impact depends on the mouse strain. Analyses of "Strain effects"
149 and "Diet effects" were performed separately, so a phosphopeptide could have both a Strain effect and
150 a StrainxDiet/Uniform Diet effect.

151 Almost half of the 441 insulin-regulated phosphopeptides displayed a Strain effect (**Fig. 2b,**
152 **Table S1**). These included phosphopeptides where C57Bl6J had a stronger insulin response than other
153 strains, such as S15 on the RNA methyltransferase Rnmt (**Fig. 2c**), and phosphopeptides where C57Bl6J
154 had a weaker insulin response, such as S48 on the vesicle fusion regulator Vamp3 (**Fig. 2d**). Vamp3
155 S48 is predicted to be highly functional (functional score = 0.750[36]), its phosphorylation correlates with
156 glucose uptake in insulin-stimulated and/or exercised human skeletal muscle[22], and Vamp3
157 overexpression rescues GLUT4 translocation in insulin resistance[37], suggesting that this site may
158 represent a genetically variable control point of GLUT4 trafficking. In general, insulin responses were
159 weaker in the four remaining strains compared to C57Bl6J, though the extent of this trend was strain-
160 dependent (**Fig. 2e**). In all, the strain-affected phosphopeptides reveal a unique fingerprint of insulin
161 signalling within each strain (**Fig. 2f**), highlighting the complex and widespread effects of genetic
162 variation on signalling networks.

163 We next examined the impact of HFD-feeding in insulin signalling. StrainxDiet effects were
164 more prevalent than Uniform diet effects (110 vs 10 phosphopeptides, **Fig. 2g, Table S1**), suggesting
165 that the molecular impact of dietary perturbation was strongly modulated by genetic background.
166 StrainxDiet effects impacted known regulatory phosphosites such as the inhibitory site S78 on Map2k4,
167 whose insulin response was attenuated by HFD-feeding only in C57Bl6J and CAST (**Fig. 2h**). Map2k4
168 activates p38 and JNK kinases which have been implicated as drivers of HFD-induced insulin
169 resistance[8], and based on the behaviour of S78, the orchestration of this detrimental signalling axis in
170 HFD-feeding may depend on genetic background.

171 HFD-feeding exerted complex effects on signalling, with the balance between suppressed and
172 enhanced insulin responses varying across strains (**Fig. 2i**). Furthermore, insulin-regulated
173 phosphopeptides were largely altered by HFD-feeding in only a single strain, and when multiple strains
174 were affected, they often changed in opposite directions (**Fig. 2j-k**). For instance, multiple insulin
175 responses were strengthened in BXH9 but weakened in C57Bl6J or CAST (**Fig. 2k**), such as S500 on
176 the translation regulator Larp4b (**Fig. S3e)**. Principal component analysis supported the highly divergent

177 impact of dietary perturbation, as HFD-feeding displaced each strain in a distinct direction in principal
178 component space (**Fig. 2l**). StrainxDiet and Strain effects were driven by a mixture of changes to
179 insulin-stimulated phosphorylation, unstimulated phosphorylation, or both, highlighting the complexity
180 of these signalling alterations (**Fig. S3f-g**). This analysis demonstrates the pervasive role of genetics in
181 shaping signalling networks, as genetic background profoundly modulated the effect of HFD-feeding
182 on insulin signalling.
183
184

185 ***Exploring genetic and dietary modulation of the insulin signalling network***

186 To understand the insulin signalling circuitry and functional pathways modulated by genetics and diet,
187 we curated a network of 160 insulin-regulated phosphosites, comprising sites from a knowledge
188 pathway-derived list of canonical insulin signalling proteins[22] and substrates of insulin-regulated
189 kinases (**Fig. 3**, see Methods). Strain and diet affected multiple highly studied signalling sites, including
190 Tsc2 S939 (Diet effect), Gsk3α S21 (Strain and Diet effects), and Tbc1d4 T649 (Strain and Diet effects),
191 while other sites such as Gsk3β S9 and Akt1s1 T247 were unaffected. Interestingly, strain and diet
192 affected both canonical and non-canonical insulin signalling proteins to a similar extent (**Fig. S3h-i**).
193 Non-canonical phosphosites could shed light on underappreciated outcomes of insulin action either
194 altered or unaffected by genetics and the environment, such as the p70S6K substrate S47 on Dnajc2
195 (Strain and Diet effects), which drives cellular senescence[38], and S315 on Pcyt1a (no Strain or Diet
196 effect), which inhibits phosphatidylcholine biosynthesis[39] (**Fig. 3**).

197 No functional pathways were overrepresented within strain or diet-affected phosphosites
198 relative to all insulin-regulated sites, implying that genetics and environment modulate most or all
199 outcomes of insulin. For instance, strain and diet affected regulatory phosphosites controlling vesicle
200 trafficking (S348, T575, S595, and T649 on the GLUT4 trafficking regulator Tbc1d4); glucose
201 metabolism (S469 and S486 on Pfkfb2, which promote glycolysis); mitochondrial structure and
202 function (S129 on Mff, which promotes mitochondrial fission); autophagy (S555 on the master
203 autophagy regulator Ulk1); gene transcription (the inhibitory site S108 on the transcription factor Tfeb);
204 and mRNA translation (S236 on ribosomal proteins S6, S422 on Eif4b, and S64 and T69 on Eif4ebp1,
205 which promote translation). Interestingly, Strain and Diet effects overlapped significantly (fold
206 enrichment = 1.50, $p = 4.40 \times 10^{-9}$, two-sided Fisher's exact test, **Fig. S3j**), implying some phosphosites
207 may be more amenable to regulation overall. As a notable exception, all six insulin-regulated
208 phosphosites on Plin1 had Diet effects while only one had a Strain effect (**Fig. 3**). Plin1 coats and
209 regulates lipid droplets, hence this enrichment of Diet effects may represent a signalling response to
210 increased intramuscular lipids in the HFD condition. Overall, genetics and environment triggered
211 widespread alterations in insulin signalling impinging on diverse cellular pathways.

212

213 ***Genetics and diet rewire insulin-regulated kinase signalling***

214 The extensive signalling changes caused by genetics and diet may result from altered kinase regulation.
215 We tested this hypothesis using a kinase substrate enrichment analysis (KSEA)[40] on phosphopeptide
216 insulin responses. KSEA accurately captured the activation of canonical insulin-regulated kinases (Akt,
217 mTOR, p70S6K, and p90RSK) and the deactivation of GSK3, confirming the validity of the approach
218 (**Fig. 4a**). Focussing on CHOW-fed mice, we identified seven kinases differentially enriched across
219 mouse strains (ANOVA adjusted p-value < 0.05, **Fig. 4b**). For example, insulin activated SGK and
220 deactivated GSK3 more in C57Bl6J and NOD than in other strains (**Fig. 4b**). Extending this analysis to
221 all mice, we identified kinases with Uniform diet or StrainxDiet effects (**Fig. 4c**). Akin to our analysis

222 of individual phosphosites (**Fig. 2**), StrainxDiet effects were more prevalent than Uniform diet effects
223 (five kinases compared to one), indicating that genetic background strongly influences the impact of
224 HFD-feeding on kinase signalling. These results suggest that the observed phosphosite signalling
225 changes could be partly due to altered insulin regulation of multiple kinases.
226
227 ***Biological variation reveals functional organisation of the insulin signalling network***
228 KSEA predicted changes in overall kinase activity, but we questioned if substrates of the same kinase
229 could be differentially regulated by genetic and environmental variation. As a case study we examined
230 substrates of Akt – a master regulator of insulin signal transduction – to assess the similarity of their
231 insulin responses across strains and diets. Strikingly, we observed a range of both positive and negative
232 correlations (**Fig. 5a**). For instance, while Tsc2 S939 and Akt1s1 T247 both activate mTORC1, their
233 insulin responses correlated poorly ($r = 0.202$, $p = 0.168$, **Fig. 5b**). Supporting these findings, similar
234 heterogeneity in Akt substrate insulin responses has previously been observed in skeletal muscle from
235 humans with differing metabolic health[41]. Hierarchical clustering revealed four distinct groups of
236 positively correlated Akt substrates (**Fig. 5a**), suggesting these groups may coordinate distinct
237 functional outputs of Akt signalling.
238 We next explored if the genetic and environmental variation in our study could reveal
239 organisational principles of the entire insulin signalling pathway. By performing weighted gene
240 correlation network analysis (WGCNA[42,43]), we identified eight subnetworks of coregulated insulin-
241 responsive phosphopeptides (**Fig. 5c**) varying in size from 16 to 120 phosphopeptides, with 91 assigned
242 to no subnetwork (**Fig. 5d, Table S3**). Examining the subnetwork "eigenpeptides" – a weighted average
243 of the constituent phosphopeptides[42,43] – revealed that the subnetworks captured distinct effects of
244 genetics and diet on insulin signalling (**Fig. 5e, Fig. S4a**). For example, HFD-feeding attenuated the
245 insulin response of subnetwork I in CAST and C57Bl6J strains (t-test adjusted $p = 0.0256$, 0.0365),
246 while subnetwork II was affected by HFD-feeding only in CAST and NOD (**Fig. 5e, Fig. S4a**, t-test
247 adjusted $p = 0.00258$, 0.0256). This suggests that the subnetworks may be sensitive to distinct cellular
248 information.
249 Next, we characterised the regulatory and functional nature of these subnetworks. Canonical
250 insulin-regulated kinases such as Akt and mTOR were enriched across multiple subnetworks (**Fig. 5f**),
251 confirming that genetic and environmental variation can reveal uncoupling of substrates targeted by the
252 same kinase (**Fig. 5a-b**). Nevertheless, visualising these subnetworks within our curated insulin
253 signalling pathway (**Fig. 3**) revealed cases where signal flowed through a single subnetwork, such as
254 from Erk2 (Y185) to its target kinase Rsk2 (T365 and S369) and Rsk2 substrates (Gab2 S211 and Nos1
255 S847) within subnetwork III (**Fig. S5**). Within multiply phosphorylated proteins, phosphosites either
256 belonged to the same subnetwork (e.g. Plin1) or diverse subnetworks (e.g. Tbc1d4 and the transcription
257 factor Nfatc2), suggesting the latter may serve as hubs integrating diverse cellular information (**Fig. S5**).

258 Some subnetworks were enriched in specific cellular compartments (GO ontologies), implying
259 that common localisation may facilitate coregulation of phosphosites (**Fig. 5g**). Coregulation may
260 partition functional outcomes of insulin action, as certain biological processes were enriched only in
261 select subnetworks (**Fig. 5h**). These included known insulin targets like "negative regulation of lipid
262 catabolic process" in subnetwork I and "positive regulation of glycogen biosynthetic process" in I, VI,
263 and VIII (**Fig. 5h**). To further probe functional differences we analysed phosphopeptide subnetwork
264 membership scores, which revealed additional pathways enriched in individual subnetworks. However,
265 these results were not significant after p-value adjustment and hence are suggestive only (**Fig. S4b-d**).
266 Lastly, we leveraged our previous phosphoproteomic time course of insulin signalling to interrogate
267 subnetwork dynamics[10] and found that phosphopeptide insulin response dynamics varied across
268 subnetworks (**Fig. 5i**). This reveals distinct temporal regulation as another feature underlying the
269 substructure of the insulin signalling network. Overall, genetic and environmental diversity illuminated
270 the complex coregulation structure of insulin signalling, featuring subnetworks that evade known
271 network circuitry and present unique functional signatures.
272
273 ***Leveraging biological variation to identify drivers of insulin responsiveness***
274 We have so far described the marked influence of genetic background and HFD-feeding on skeletal
275 muscle insulin signalling, evident at the level of individual phosphosites, protein kinases, and co-
276 regulated network modules. We hypothesised that by associating this signalling diversity with a
277 phenotypic output of insulin, such as enhanced glucose uptake, we would filter out mechanistically
278 irrelevant phosphosites and hence prioritise molecular regulators of the phenotype. To test this
279 hypothesis, we measured *in vivo* glucose uptake with ^{3}H-2DG tracer in the same muscle samples used
280 for phosphoproteomics. Insulin-stimulated glucose uptake differed by more than twofold across strains
281 (two-way ANOVA strain effect $p = 4.78 \times 10^{-7}$) and was almost uniformly decreased by HFD-feeding
282 (two-way ANOVA diet effect $p = 1.83 \times 10^{-5}$) (**Fig. 6a**). This highlights that genetic background and
283 dietary status are key determinants of insulin responsiveness.
284 To prioritise signalling nodes responsible for differences in insulin responsiveness, we correlated
285 all insulin-regulated phosphopeptides with glucose uptake in insulin-stimulated muscles, resulting in
286 37 significantly correlated phosphopeptides ($r > 0.35$ or < -0.35, q-value < 0.1, **Fig. 6b**). The most
287 significantly correlated phosphopeptide contained T1174 and S1176 on the nitric oxide synthase Nos3.
288 The latter serves as a positive control for our analysis, as this site is known to be phosphorylated in
289 response to insulin to promote *in vivo* glucose uptake by vasodilation[44–46] (**Fig. 6c**). Other correlated
290 phosphopeptides that could modulate insulin responsiveness include S1751 on Afdn, a phosphosite
291 implicated in insulin action[47], and S196 on the Prkag2 subunit of AMPK, a major metabolic signalling
292 hub promoting glucose uptake[48] (**Fig. 6b**). These examples suggest that our analysis prioritised
293 regulators of glucose uptake.

While the above analysis identified phosphosites associated with glucose uptake through their absolute abundance, we hypothesized that for some phosphosites, the magnitude of their response to insulin may be a stronger determinant of insulin action. We found that the insulin response values of 13 phosphopeptides correlated with insulin-stimulated glucose uptake ($r > 0.35$ or < -0.35, q-value < 0.1, **Fig. 6d**). These were largely distinct from the 37 phosphopeptides identified in our first analysis, indicating that the two approaches captured complementary information. Several of these phosphopeptides could regulate insulin-stimulated glucose uptake, such as the regulatory site S469 on the enzyme Pfkfb2 which activates glycolysis, a major pathway for glucose consumption[49–51] (**Fig. 6e**), and S177 on Rcsd1, which could affect GLUT4 vesicle transport via actin cytoskeleton remodelling[52] (**Fig. 6d**). The associations identified in these analyses could arise uniquely at the level of protein phosphorylation or could be driven by changes in total protein abundance. To assess this, we mined soleus total proteomics data from a recent study of seven CHOW and HFD-fed mouse strains, three of which were in common with this study (C57BL6J, BXH9, BXD34)[18]. Of the 34 glucose uptake-associated phosphoproteins we identified, 16 were quantified in both studies and only two additionally correlate with glucose uptake at the total protein level (Ppp6r1 and Ttn, **Fig. S6a**). Hence, it seems likely that most glucose uptake-phosphosite associations were not driven by protein abundance changes, underscoring the utility of phosphoproteomics to provide unique information on top of more classical omics layers.

In addition to individual phosphosites, the status of larger signalling network components could also influence insulin responsiveness. Kinase enrichment scores affected by strain or diet did not correlate with glucose uptake (**Table S4**), suggesting insulin action is not dominated by the net activity of specific kinases. Interestingly, two WGCNA-derived insulin signalling subnetworks correlated with glucose uptake: subnetwork V ($r = 0.436$, $p = 0.00173$) and subnetwork I ($r = 0.332$, $p = 0.0197$, **Fig. 6f**). Subnetwork V could modulate glucose uptake through actin cytoskeleton remodelling via Rscd1 S177, through glucose metabolism promotion via Gys1 S641 (**Table S3**), and by influencing GLUT4 vesicle trafficking due to its enrichment at "cytoplasmic vesicle membranes" (**Fig. 5g**). It was also enriched in substrates of GSK3, which has been implicated in insulin resistance in skeletal muscle[53–55] and adipose tissue[32]. Subnetwork I, the largest cluster containing 27% of insulin-regulated phosphopeptides, was enriched in multiple kinases and biological processes (**Fig. 5f, h**), suggesting it may be a central regulatory hub for various outcomes of insulin action including glucose uptake. Examining the subnetwork membership scores for glucose-uptake correlated phosphopeptides also revealed a preference for clusters V and I, supporting this analysis (**Fig. S6b-c**). Overall, compartmentalisation of insulin-responsive phosphosites into subnetworks may enable independent control of insulin's functional outputs, since only two subnetworks correlated with insulin-stimulated glucose uptake.

331 ***Upregulating glycolysis reverses insulin resistance***

332 We next aimed to validate our approach for identifying regulatory mechanisms of insulin-stimulated
333 glucose uptake. S469 on Pfkfb2 correlated highly with glucose uptake follow insulin stimulation (**Fig.**
334 **6e**). Phosphorylation of this site leads to increased production of F2,6BP, a potent glycolytic agonist,
335 suggesting that activating glycolysis may play a key role in muscle insulin responsiveness. This is
336 consistent with our previous findings that glycolytic enzyme abundance was strongly associated with
337 *ex vivo* insulin-stimulated glucose uptake in muscle from inbred mice[18], that the insulin resistance-
338 reversing small molecule thiostrepton enhances glycolytic capacity[56], and that decreasing glycolytic
339 flux caused insulin resistance *in vitro*[57]. To further establish glycolysis as a regulator of insulin
340 responsiveness in skeletal muscle, we decided to investigate whether upregulating glycolysis through
341 F2,6BP production can restore insulin-stimulated glucose uptake in insulin resistance.

342 Since Pfkfb2 requires phosphorylation by Akt to produce F2,6BP substantially, increasing
343 F2,6BP production via Pfkfb2 would require enhanced activating site phosphorylation, which is
344 difficult to achieve in a targeted fashion, or phosphomimetic mutation of activating sites to
345 aspartate/glutamate, which often does not recapitulate the molecular effects of serine/threonine
346 phosphorylation[58]. By contrast, the paralog Pfkfb3 has high basal production rates and lacks an Akt
347 motif at the corresponding phosphosites[51]. We therefore rationalised that overexpressing Pfkfb3 would
348 robustly increase F2,6BP production and enhance glycolysis regardless of insulin stimulation and Akt
349 signalling (**Fig. 6g**). To avoid systemic effects of Pfkfb3 overexpression we studied cultured L6-
350 GLUT4-HA myotubes, which display robust insulin regulation of GLUT4 trafficking and develop
351 insulin resistance upon palmitate treatment, mimicking lipotoxicity, a trigger of *in vivo* insulin
352 resistance[59]. While L6 cells are of rat origin, they are preferable to the popular C2C12 mouse cell line
353 since the latter lack an insulin-responsive vesicular compartment[60] and undergo spontaneous contraction,
354 resulting in confounding non-insulin dependent glucose uptake[61].

355 As anticipated, Pfkfb3 overexpression increased glycolytic capacity in L6-GLUT4-HA myotubes
356 as measured by extracellular acidification rate (**Fig. S7a-c**). Pfkfb3 overexpression also restored insulin-
357 responsive glucose uptake to normal levels in palmitate-treated cells (**Fig. 6h, Fig. S7d**). This effect
358 was only observed in cells treated with palmitate and insulin, suggesting it specifically modulated
359 insulin action rather than non-specifically increasing glucose uptake through enhanced glucose
360 consumption (**Fig. S7d**). This may be due to enhanced insulin signalling, as we have previously
361 observed that transient Pfkfb3 overexpression increased Akt signalling in HEK293 cells[57]. However,
362 immunoblotting of canonical insulin-responsive phosphosites on Akt and its substrates GSK3α/β and
363 PRAS40 revealed minimal effect of palmitate treatment and Pfkfb3 overexpression (**Fig. S7e-f**), hence
364 more detailed phosphoproteomics studies are needed to clarify whether Pfkfb3 overexpression restored
365 insulin action by modulating insulin signalling. Overall, our results further establish glycolytic flux as
366 a major determinant of the glucose uptake arm of muscle insulin action and highlight the power of
367 studying phosphoproteomics across the gene-by-environment landscape to identify causal drivers of

368 complex phenotypes. We anticipate that our catalogue of glucose uptake-correlated phosphosites will
369 provide a rich starting point for future investigations into mechanisms of insulin action and resistance.

Discussion

The environment shapes the flow of information from genotype to phenotype. Many studies have interrogated the role of intermediate molecular layers such as the transcriptome or proteome, however few studies have examined how protein post-translation modifications participate in this information transfer. Here we have approached this problem by leveraging diverse inbred mouse strains and phosphoproteomics to examine the insulin signalling network across a landscape of genetic and dietary variation. Genetic background significantly altered the insulin signalling network both independently and in concert with dietary status, affecting myriad phosphosites and multiple kinases. We exploited this variation in signalling responses in two ways – to study the partitioning of the Akt and insulin signalling pathways into distinct subnetworks of coregulated phosphosites; and to identify potential regulators of insulin responsiveness by associating phosphorylation with insulin-stimulated glucose uptake. Finally, validation studies in L6 myotubes confirmed the major role of accelerated glycolysis as a key regulator of insulin responsiveness.

Genetic and diet-driven signalling changes did not transmit linearly through our current model of the insulin signalling network, illustrating that this model remains incomplete. Notably, substrates of kinases such as Akt clustered into distinct groups based on differing insulin responses. Hence, it is an oversimplification to model signalling pathways as networks of individual kinases since substrates of the same kinase display independent regulation. This could arise from localisation of a kinase to distinct substrate pools[62–64]; interactors targeting a kinase to different substrates[62]; substrate phosphorylation by alternate kinases[65]; the dephosphorylation of specific substrates by phosphatases; kinase post-translational modifications altering substrate specificity; and distinct substrate phosphorylation kinetics[10]. As our knowledge of the repertoire of kinase substrates continues to deepen[66], future research should explore how the above mechanisms contribute to finer regulation of these substrates. Genetic and environmental variation also exposed a coregulation subnetwork structure within the insulin signalling network. The enrichment of subnetworks in distinct biological processes, and the selective association of two subnetworks with glucose uptake, suggests that this coregulation structure may direct independent control of distinct outcomes of insulin action. This exciting possibility necessitates further investigation, including replication in independent cohorts and spatiotemporal characterisation of subnetwork dynamics. Alternatively, one could overlap subnetworks with genetic information, such as genes associated with glucose homeostasis and other metabolic traits in human GWAS studies[67], or muscle-specific eQTLs or pQTLs genetically colocalised with similar traits[68], to further prioritise subnetwork-associated phenotypes and identify potential drivers within subnetworks.

Muscle insulin signalling responses vary across individuals[22,41], and our results suggest that baseline genetic differences and an individual's environment both alter signalling, with the environment's influence depending strongly on genetic background. Signalling pathways are popular therapeutic targets due to their importance in human health and the relative ease of pharmaceutical interventions[69]. Our results advocate for a personalised approach to such therapies, implying that the

407 efficacy of treatments aiming to correct pathological signalling responses will depend on an individual's
408 genetic background. In cancer, where signalling networks are dysregulated heterogeneously, modelling
409 patient-specific networks has already shown promise for identifying personalised drug targets[70,71].
410 Personalised medicine approaches will also be aided by a comprehensive understanding of how genetics
411 shape signalling networks and potentiate their modulation by the environment. Recent studies have
412 made the first step, revealing that the ground-state phosphoproteome can be altered by mutations
413 affecting network components such as kinases, phosphatases, and phosphoproteins, as well as the
414 molecular milieu the network is exposed to including extracellular signalling ligands[20,21]. An important
415 corollary of such genetic factors is that multiple genetic backgrounds should be studied when
416 establishing generalizable signalling responses. Our data indicate that insulin responses in C57BL6J –
417 the most commonly studied mouse strain – are not necessarily generalizable, indicated by phosphosites
418 such as S15 on Rnmt that were insulin regulated almost exclusively in C57Bl6J.

419 A major challenge in studying signal transduction with omics technologies is that hundreds to
420 thousands of molecular events typically respond to a cellular signal, making it difficult to pinpoint the
421 most crucial regulatory nodes. To tackle this challenge, we previously demonstrated that associating
422 phosphoproteomics with physiological phenotypes across diverse individuals enriches for phosphosites
423 more likely to modulate biological responses[22]. Here we have elaborated on this approach, revealing
424 that associating phosphorylation with phenotype across a genetic and environmental landscape can
425 identify regulators of specific biological processes, such as insulin-stimulated glucose uptake. Our
426 results recapitulated known glucose uptake regulators and led to further validation of glycolytic flux as
427 a modulator of insulin responsiveness. We have previously demonstrated that reduced glycolytic flux
428 impairs GLUT4 translocation and insulin signalling[57], implying that the status of glycolysis is sensed
429 by proteins regulating insulin action. An enhanced glycolytic metabolic tone may alter production of
430 reactive oxygen species, a known modulator of insulin action[59,72,73] and insulin signalling[74].
431 Alternatively, recent approaches to map protein-metabolite interactions could identify points of
432 allosteric crosstalk between glycolytic metabolites and insulin action proteins[75,76], hence broadening our
433 understanding of the bidirectional communication between insulin action and metabolism.

434 It was striking that only several dozen insulin-regulated phosphopeptides associated significantly
435 with glucose uptake. Since insulin triggers multiple distinct cellular outcomes, it is possible that only a
436 subset of insulin-responsive phosphosites contribute to enhanced glucose uptake. Moreover, many of
437 these phosphosites might only be permissive for insulin-stimulated glucose uptake and are not major
438 regulatory nodes determining the fidelity of the process. For example, while mutation of the four
439 primary Akt regulatory sites on Tbc1d4 blocks GLUT4 translocation[77], none of these phosphosites
440 featured strong positive correlations with glucose uptake in our analysis (**Fig. S8**). This implies that
441 their phosphorylation may promote glucose uptake in a functionally permissive, switch-like fashion.
442 We suggest that the glucose uptake-associated phosphosites we have identified will be enriched in major

443 regulators of insulin responsiveness, necessitating future functional studies to characterise these sites
444 and explore their involvement in insulin resistance.
445 Our work demonstrates that genetic and environmental variation can profoundly modulate global
446 signalling networks and that the influences of these factors are intrinsically entwined. We show that the
447 resulting diversity in signalling responses can be leveraged to pinpoint regulators of insulin-stimulated
448 glucose uptake, providing a powerful methodological framework for interrogating the regulatory basis
449 of complex biological pathways.
450
451 ***Limitations of this study***
452 First, this study focused on male mice and examined only five inbred strains. This limited number of
453 strains may mean that our association analysis was underpowered to detect some regulators of insulin
454 responsiveness. Importantly, however, this does not imply that the regulators identified are incorrect,
455 but only that there may be more to discover with larger cohorts. In addition, studies incorporating male
456 and female subjects found that mouse insulin sensitivity was affected by interactions between sex and
457 strain[78], and insulin signalling in stem cell-derived myoblasts by interactions between sex and donor
458 metabolic health[31]. Hence, we anticipate that sex would contribute another important dimension to the
459 web of interactions between genetics, diet, and insulin signalling identified here. Future work should
460 therefore extend our approach across a broader range of genetic backgrounds, as well as in female mice.
461 Second, we only examined insulin signalling after 10 minutes, since measuring multiple timepoints
462 would have drastically increased the number of animals and samples required. Integration of dynamic
463 phosphoproteome data from cultured cells indicated that insulin signalling dynamics may contribute to
464 trends in our data (**Fig. 5i**), suggesting the exploration of signalling at additional timepoints may be
465 fruitful in the future.
466 Third, mammalian tissues are a heterogeneous mixture of cell types, and differences in this
467 mixture could result in different signalling responses measured at the whole tissue level. In our
468 experience, the soleus can be reproducibly dissected as an intact muscle with little contamination from
469 surrounding tissues, making it unlikely that cell type composition varied across samples due to tissue
470 collection. However, we cannot exclude the possibility that differences in the composition of the soleus
471 muscle across strains and diets contributed to the signalling changes we detected. We were also unable
472 to determine the extent to which signalling changes arose from muscle-intrinsic or extrinsic factors. For
473 instance, body weight varied substantially across mice and correlated significantly with 25% of Strain
474 and Diet-affected phosphopeptides (**Fig. S8c**), suggesting obesity-related systemic factors likely impact
475 a subset of the muscle insulin signalling network. Furthermore, genetic differences in lifespan could
476 alter the "biological age" of different strains and their phosphoproteomes, though we could not assess
477 this possibility since lifespan data is not available for most strains used. Lastly, as we did not perform
478 total proteomics, we did not assess whether phosphosite changes were caused by differences in total
479 protein abundance. However, since protein abundance should not change within a 10-minute insulin

stimulation[32], the acute insulin responses we observed should only reflect differences in protein phosphorylation. Furthermore, in our previous studies of insulin signalling in adipocytes[32] or human skeletal muscle[22] in which deep proteomes were measured in parallel, we found little global correlation between changes in protein phosphorylation and protein abundance across experimental conditions regardless of insulin stimulation, suggesting the contribution of protein abundance to phosphosite changes across strains and diets was likely minimal.

Additional information

Acknowledgements

D.E.J. is an Australian Research Council (ARC) Laureate Fellow. The content is solely the responsibility of the authors and does not necessarily represent the official views of the ARC. The authors also acknowledge the facilities, and the scientific and technical assistance of the Sydney Mass Spectrometry Facility and the Laboratory Animal Services at the Charles Perkins Centre, University of Sydney.

Author Contributions

Conceptualization: JvG, SWCM, SJH, DEJ. Methodology: JvG, HBC, SWCM, ADV, MP, SJH. Formal analysis: JvG. Investigation: JvG, SWCM, HBC, ADV, MP, JS, SM, MEN, SJH. Resources: JS. Writing – Original Draft: JvG. Writing – Review and Editing: All authors. Visualization: JvG. Supervision: SWCM, SJH, DEJ. Project Administration: JvG, SWCM, SJH, DEJ. Funding Acquisition: DEJ

Declaration of Interests

The authors declare no competing interests.

Data Access Statement

All raw and Spectronaut processed phosphoproteomics data have been deposited in the PRIDE proteomeXchange repository and will be made publicly available upon publication. Processed data are available as supplementary tables.

Code availability

All code used to analyse data and produce figures has been uploaded to https://github.com/JulianvanGerwen/GxE_muscle_phos

Methods

Statistical analysis

517 Most statistical analysis was performed in the R programming environment using RStudio (R version:
518 4.2.1, RStudio version: 2022.07.1 Build 554). Analysis of GLUT4-HA-L6 myotube Pfkfb3 expression,
519 2DG uptake, and ECAR was performed in GraphPad Prism (version: 9.3.1).
520
521 ***Animal details***
522 Male C57BL/6J (C57Bl6J), BXH9/TyJ (BXH9), BXD34/TyJ (BXD34), and CAST/EiJ (CAST) mice
523 were purchased from Australian BioResources (Moss Vale, NSW, Australia) while NOD/ShiLtJ (NOD)
524 mice were purchased from Animal Resources Centre (Murdoch, WA, Australia). Mice were at most 9
525 weeks old upon arrival. Mice were housed at 23 °C on a 12 h light/dark cycle in cages of 2-5, with free
526 access to food and water. At 12-16 weeks of age mice were randomly allocated to a standard CHOW
527 diet (13% calories from fat, 65% from carbohydrate, 22% from protein; "Irradiated Rat and Mouse
528 Diet", Specialty Feeds, Glen Forrest, WA, Australia) or a high-fat high-sucrose diet made in house
529 (HFD; 45% calories from fat (40% calories from lard), 35% from carbohydrate (14% calories from
530 starch), and 22% from protein) and sacrificed exactly 6 weeks later. The number of mice in each group
531 are C57Bl6J: 8 CHOW, 10 HFD; NOD: 10 CHOW, 10 HFD; BXH9: 8 CHOW, 9 HFD; CAST: 9
532 CHOW, 9 HFD; BXD34: 10 CHOW, 11 HFD. Procedures were carried out with approval from the
533 University of Sydney Animal Ethics Committee following guidelines issued by NHMRC (Australia).
534
535 ***Assessment of body composition***
536 Body composition of individual mice was assessed using the EchoMRI-900 to determine lean mass 1
537 day before a glucose tolerance test and 5-6 days before euthanasia. Analysis was performed as per the
538 manufacturer's specifications.
539
540 ***Glucose tolerance test***
541 On the day of a glucose tolerance test mice were fasted for 6 h (0800-1400). Mice were then orally
542 gavaged with 20% (w/v) glucose in water at 2 g/kg lean mass, and blood glucose was measured from
543 the tail vein using a glucometer 0, 15, 30, 45, 60, and 90 min after the gavage. At 0 and 15 min, 5 µL
544 blood was also collected into an Insulin Mouse Ultra-Sensitive ELISA plate (Crystal Chem USA, Elk
545 Grove Village, Illinois, USA). Blood insulin concentration was measured according to the
546 manufacturer's protocol, using linear extrapolation from an insulin standard curve. The area of the blood
547 glucose curve (AOC) was calculated by:

548 $$\mathrm{AOC} = \sum_{i=2}^{n} \frac{(G_{i-1} - G_1) + (G_i - G_1)}{2}(t_i - t_{i-1})$$

549 Where i represents the ith timepoint at which blood glucose was measured, n represents the last
550 timepoint, t_i represents the time (min) of the ith timepoint, and G_i represents blood glucose
551 concentration (mM) at the ith timepoint.
552

553 ***In vivo insulin stimulation***

554 On the day of the procedure mice were fasted for 2h (1100-1300). Mice were then anaesthetised by
555 intraperitoneal injection of sodium pentobarbital at 80 mg/kg body mass. To counter anaesthesia-
556 associated declines in body temperature, mice were wrapped in aluminium foil and placed on a heating
557 pad at 37°C. After 15 min anaesthesia, mice were injected retro-orbitally as previously described[79] with
558 50 µL plasma replacement (B. Braun, Melsungen, DEU) containing 10 µCi ^{3}H-2DG and saline or
559 insulin (0.75 U/kg lean mass). Blood glucose was measured from the tail vein using a glucometer
560 (AccuCheck, Roche Diabetes Care, NSW, Australia) 1 min prior to injection and 1, 5, 7.5, and 10 min
561 after injection. Simultaneously, 5 µL blood was collected into 95 µL 0.9% NaCl on ice to measure ^{3}H-
562 2DG blood concentration. Ten minutes after insulin injection mice were sacrificed by cervical
563 dislocation and the soleus muscle was rapidly excised, immediately frozen in liquid nitrogen, and stored
564 at -80°C. To measure ^{3}H-2DG blood concentration, diluted blood samples were first centrifuged at
565 10,000 xg for 10 min to pellet blood cells. Supernatant (70 µL) was collected and combined with 3 mL
566 liquid scintillation cocktail (Perkin Elmer, Massachusetts, USA: 6013321) to allow the measurement of
567 ^{3}H with a Tri-Carb 2810TR Liquid Scintillation Counter (Perkin Elmer, Massachusetts, USA).
568

569 ***Skeletal muscle lysis***

570 Frozen muscle tissue was powdered by grinding in a mortar and pestle chilled with liquid nitrogen and
571 dry ice. To lyse powdered tissue, 200 µL lysis buffer (4% (w/v) sodium deoxycholate, 100 mM Tris-
572 HCl pH 8.5) was added followed by 10 s vortexing. Samples were then sonicated at 4 °C at 90% power
573 using pulses of 2 s on, 5 s off for a total time of 1 min. Samples were then immediately boiled at 95 °C
574 with 1,500 rpm shaking for 5 min and sonicated for a further 2 min (4 °C, 90% power, 5 s on and 5 s
575 off) to ensure complete lysis. Lysate was then centrifuged at 20,000 xg for 5 min and 180 µL supernatant
576 was collected. Cysteine residues were reduced and alkylated by adding 40 mM chloroacetamide and 10
577 mM TCEP at pH 7. Lysate was incubated for 5 min at 45 °C with 1,500 rpm shaking and then incubated
578 for a further 40 min at room temperature without shaking.

579 Next, 800 µL 100% chloroform and 1,600 µL 100% methanol were added following 30 s
580 sonication at 90% power. LC/MS grade water (800 µL) was added following 5 min mixing at 1,000
581 rpm. Lysate was centrifuged for 5 min at 2,000 xg to induce a phase separation. The majority of the
582 aqueous phase (2,400 µL) was removed and 2,000 µL was reserved for ^{3}H-2DG quantification. Next,
583 2,400 µL 100% methanol was added following 30 s mixing at 800 rpm and centrifugation at 2,000 xg
584 for 5 min. The supernatant was discarded, and the protein pellet was air-dried for 5 min. Protein was
585 reconstituted in 200 µL lysis buffer, sonicated at 60% power for 15 s using a tip-probe sonicator and
586 boiled for 5 min in a thermomixer at 95 °C with 1,500 rpm shaking.
587

588 ***Determining ^{3}H-2DG uptake into muscle tissue***

589 Anion exchange chromatography was used to quantify ^{3}H-p2DG, representing ^{3}H-2DG that has been
590 taken up by cells. For quantification of total (phosphorylated and unphosphorylated) ^{3}H-2DG, 375 µL
591 lysate aqueous phase was combined with 1,125 µL water and reserved. For quantification of
592 unphosphorylated ^{3}H-2DG, 1,000 µL lysate aqueous phase was added to 300 µL 37.5% (w/v) AG 1-
593 X8 anion exchange resin (Bio-Rad, Hercules, CA, USA: 1401441) and washed with 3 mL water to
594 remove p2DG. Liquid scintillation cocktail (3 mL) was then added to 1,500 µL total and
595 unphosphorylated ^{3}H-2DG solutions, and ^{3}H-2DG was measured using a Tri-Carb 2810R Liquid
596 Scintillation Counter. Unphosphorylated and total ^{3}H-2DG scintillation counts were subtracted to
597 quantify ^{3}H-p2DG.
598 ^{3}H-2DG blood concentration at 1, 5, 7.5, and 10 min after injection was fit to an exponential
599 curve $y = C_p(0)e^{-K_p t}$ where $C_p(0)$ represents the predicted initial tracer concentration (DPM/µL) and
600 K_p represents the rate of tracer disappearance from the blood (1/min), to model the disappearance of
601 ^{3}H-2DG from the blood as it is taken up and trapped by peripheral tissues[80]. $C_p(1)$ was removed when
602 it was abnormally low ($C_p(1) < C_p(5),\ C_p(5) - C_p(1) > 0.5 \times (C_p(5) - C_p(7.5))$), which likely
603 indicates insufficient diffusion of circulating ^{3}H-2DG into the tail vein. To account for different rates
604 of blood ^{3}H-2DG disappearance across mice, ^{3}H-2DG uptake was calculated as a rate constant[80]:

605 $$K_i = \frac{C_i(t)K_p}{C_p(0)(1 - e^{-K_p t})}$$

606 Where t represents the time after injection that the animal was sacrificed (min) and $C_i(t)$ represents the
607 concentration of ^{3}H-p2DG in the tissue harvested at time t (DPM/mg tissue).
608
609 ***Phosphoproteomics sample preparation***
610 Phosphopeptides were isolated using the EasyPhos protocol[28] with minor modifications. Protein
611 (C57Bl6J and NOD: 755 µg, BXH9 and BXD34: 511 µg, CAST: 364 µg) was digested into peptides
612 by incubation in 1% (w/w) Trypsin and LysC on a thermomixer at 37°C with 1,500 rpm shaking for 14
613 h. Following digestion, 400 µL 100% isopropanol and 100 µL EasyPhos enrichment buffer (48% (v/v)
614 TFA, 8 mM KH_2PO_4) were sequentially added with mixing (1,500 rpm, 30 s) after each addition. Lysate
615 was centrifuged at 20,000 xg for 15 min to pellet insoluble material and transferred to a deep well plate.
616 The EasyPhos protocol was then followed from step 12[28].
617
618 ***Liquid chromatography-tandem mass spectrometry (LC-MS/MS)***
619 Enriched phosphopeptides in MS loading buffer (2% ACN, 0.3% TFA) were loaded onto in-house
620 fabricated 55 cm columns (75 µM I.D.), packed with 1.9 µM C18 ReproSil Pur AQ particles (Dr.
621 Maisch HPLC GmbH, Ammerbuch, DEU) with a Dionex U3000 HPLC (Thermo Fisher Scientific),
622 interfaced with an Orbitrap Exploris 480 mass spectrometer (Thermo Fisher Scientific). Column
623 temperature was maintained at 60°C using a column oven (Sonation lab solutions, Biberach, DEU), and
624 peptides were separated using a binary buffer system comprising 0.1% formic acid (buffer A) and 80%

625 ACN plus 0.1% formic acid (buffer B) at a flow rate of 400 nL/min. A gradient of 3–19% buffer B was
626 employed over 40 min followed by 19–41% buffer B over 20 min, resulting in approximately 1 h
627 gradients. Peptides were analysed with one full scan (350–1,400 m/z, R = 120,000) at a target of $3e^6$
628 ions, followed by 48 data-independent acquisition MS/MS scans (350–1,022 m/z) with higher-energy
629 collisional dissociation (target $3e^6$ ions, max injection time 22 ms, isolation window 14 m/z, 1 m/z
630 window overlap, normalised collision energy 25%), and fragments were detected in the Orbitrap (R =
631 15,000).
632
633 ***MS raw data processing***
634 Raw spectral data were analysed using Spectronaut (v16.0.220606.53000). Data were searched using
635 directDIA against the Mouse UniProt Reference Proteome database (January 2022 release), with default
636 settings (precursor and protein Qvalue cutoffs 0.01, Qvalue filtering, MS2 quantification), with "PTM
637 localization" filtering turned on (threshold 0.5), and the inbuilt peptide collapse function.
638
639

640 ***Phosphoproteomics data processing***

641 Phosphopeptide intensities were log2 transformed and median normalised. Non-class I phosphopeptides
642 (localisation score ≤ 0.75) were then removed. Finally, for each phosphopeptide, outlier values were
643 removed that had a log2 intensity < 5 and were > 6 log2 intensity units lower than the phosphopeptide
644 median. Log2 fold changes between conditions were computed using condition medians.

645

646 ***Identifying insulin-regulated phosphopeptides***

647 To allow comparison across conditions, phosphopeptides were filtered for those highly quantified in
648 most strain-diet combinations. For a given phosphopeptide, this filtering was performed on two levels.
649 Firstly, each of the 10 strain-diet combinations were retained if there were ≥ 3 insulin-stimulated values
650 and ≥ 3 unstimulated values. Then, the phosphopeptide itself was retained if ≥ 8 strain-diet combinations
651 had passed the previously filtering. Phosphopeptides were then fit to a three-way ANOVA with all
652 interaction terms ("aov" in the R package "stats") and an F-test was performed assessing the main effect
653 of insulin stimulation. To correct for multiple hypothesis testing p-values were converted into q-values
654 (R package "qvalue"[81]). The log2(insulin/unstimulated) fold change with the greatest magnitude across
655 strain-diet combinations was then calculated (max log2(insulin/unstimulated)). Phosphopeptides were
656 considered "insulin-regulated" when q < 0.05 and if insulin increased or decreased phosphorylation by >
657 1.5-fold in at least one strain-diet combination (max log2(insulin/unstimulated) > 0.58 or < -0.58).

658

659 ***Calculation of insulin response values***

660 For all phosphopeptides the distribution of "insulin responses" in each strain-diet combination was
661 calculated. Specifically, within each strain-diet combination all insulin-stimulated values were
662 normalised by subtracting the unstimulated median.

663

664 ***Identifying strain and diet effects***

665 *Strain effects*

666 For each insulin-regulated phosphopeptide a one-way ANOVA was performed modelling the insulin
667 response as a function of mouse strain within the CHOW diet. p-values were converted to q-values.
668 For significant phosphopeptides (q < 0.05), t-tests were performed comparing the insulin response of
669 C57Bl6J to each of the other four strains. t-test p-values were converted to q-values and considered
670 significant when q < 0.05. To ensure that significant differences between a strain and C57Bl6J were
671 of a meaningful magnitude, the strain's log2(insulin/unstimulated) was compared to the C57Bl6J
672 log2(insulin/unstimulated). In general, if the absolute difference between the two was greater than
673 0.58 this was accepted. However, this threshold was decreased for phosphopeptides with weaker
674 insulin regulation. Specifically, the difference was retained if it passed the following filtering:

675

$$Strain\ log2(insulin/unstimulated) > f(C57Bl6J\ log2(insulin/unstimulated))$$
or
$$Strain\ log2(insulin/unstimulated) < g(C57Bl6J\ log2(insulin/unstimulated)),$$
where $f(x)$ and $g(x)$ are defined as:

$$f(x) = \left\{ \begin{array}{ll} x + 0.58, & \text{if } x \geq 2 \times 0.58 \\ \frac{5}{4}x + \frac{1}{2} \times 0.58, & \text{if } 0 \leq x < 2 \times 0.58 \\ x + \frac{1}{2} \times 0.58, & \text{if } -\frac{1}{2} \times 0.58 \leq x < 0 \\ \frac{4}{5}x + \frac{2}{5} \times 0.58, & \text{if } -3 \times 0.58 \leq x < -\frac{1}{2} \times 0.58 \\ x + 0.58, & \text{if } x < -3 \times 0.58 \end{array} \right\}$$

$$g(x) = \left\{ \begin{array}{ll} x - 0.58, & \text{if } x \geq 3 \times 0.58 \\ \frac{4}{5}x - \frac{2}{5} \times 0.58, & \text{if } \frac{1}{2} \times 0.58 \leq x < 3 \times 0.58 \\ x - \frac{1}{2} \times 0.58, & \text{if } 0 \leq x < \frac{1}{2} \times 0.58 \\ \frac{5}{4}x - \frac{1}{2} \times 0.58, & \text{if } -2 \times 0.58 \leq x < 0 \\ x - 0.58, & \text{if } x < -2 \times 0.58 \end{array} \right\}$$

An insulin-regulated phosphopeptide was considered to have a "Strain effect" if the insulin response in at least one strain was different to C57Bl6J using the q-value and log2 fold-change criteria described above.

Uniform diet and StrainxDiet effects

For each insulin-regulated phosphopeptide a two-way ANOVA was performed modelling the insulin response as a function of strain, diet, and their interaction. The p-values for the Diet and StrainxDiet terms were converted to q-values. Whenever the StrainxDiet term was significant ($q < 0.05$), additional tests were performed to identify specific strains in which the insulin response differed between CHOW and HFD. If the StrainxDiet term was not significant but the Diet term was significant, a separate filtering procedure was performed.

When the StrainxDiet term was significant, t-tests were performed to compare the CHOW insulin response to the HFD insulin response within each strain. When a t-test was significant ($q < 0.05$), the log2(insulin/unstimulated) filtering procedure described for "Strain effects" was applied comparing CHOW and HFD fold changes. Insulin-regulated phosphopeptides were considered to have a "StrainxDiet effect" if there was a difference between CHOW and HFD in at least one strain.

When only the Diet term was significant, the log2(insulin/unstimulated) filtering procedure described for "Strain effects" was applied, comparing the mean log2(insulin/unstimulated) across strains within CHOW, to the mean across HFD. Insulin-regulated phosphopeptides that passed this filter were considered to have a "Uniform diet effect".

699 ***Curated insulin signalling subnetwork***

700 A subnetwork of insulin-regulated phosphosites was curated by compiling all sites on proteins from a
701 previously published knowledge pathway-derived list of canonical insulin signalling proteins[22]. Several
702 phosphosites and proteins that were not detected as insulin regulated were included due to their
703 importance in the insulin signalling pathway. Additionally, all *in vivo* substrates of canonical insulin-
704 regulated kinases (Akt, mTOR, AMPK, Raf, Mek1/2, Erk1/2, p90RSK/Rsk2, p70S6K, Pdk1, INSR)
705 annotated in PhosphositePlus were included[33]. Annotations from orthologous phosphosites were pooled
706 across species using PhosphositePlus Site Group IDs. Phosphosite regulatory roles from
707 PhosphositePlus were indicated after manual validation by literature search. Proteins were assigned to
708 functional groups (e.g. mRNA processing, lipid metabolism) based on their Uniprot descriptions.

709

710 ***Kinase substrate enrichment analysis***

711 Kinase-substrate annotations were collated from PhosphositePlus and mapped into phosphoproteomics
712 data using Site Group IDs. Only annotations supported by *in vivo* evidence were used. Annotations for
713 kinase isoforms (e.g. Akt1, Akt2, Akt3) were merged. Substrate annotations for GSK3 were
714 supplemented with a recent list of 274 putative GSK3 substrates determined by phosphoproteomics and
715 motif analysis[32]. Autophosphorylation sites and promiscuous phosphosites targeted by ≥ 4 kinases were
716 removed. Kinase substrate enrichment analysis (KSEA) was then performed with the "ksea" function
717 from the R package "ksea"[40] (version: 0.1.2) using insulin response data and 1,000 permutations to
718 determine empirical p-values. Only phosphopeptides quantified in ≥ 50% of samples and with ≥ 1
719 insulin response value in all strain-diet combinations were used. In each sample kinases with < 5
720 quantified substrates were excluded, and only kinases with significant enrichment ($p < 0.05$) in ≥ 5
721 samples were used in subsequent analysis. To identify Strain effects on kinase activity, one-way
722 ANOVAs were performed on CHOW KSEA enrichment scores. To identify Uniform diet or
723 StrainxDiet effects, two-way ANOVAs were performed on KSEA enrichment scores testing the effects
724 of strain, diet, and their interaction. p-values were adjusted by the Benjamini-Hochberg procedure.

725

726 ***Insulin signalling subnetwork analysis***

727 Weighted gene correlation network analysis (WGCNA[42,43]) was performed with the
728 "blockwiseModules" function from the R package "WGCNA" (version 1.71) using the insulin
729 response values of all insulin-regulated phosphopeptides. Default parameters were used except for
730 power = 3 (determined as recommended in [42]), deepSplit = 3, minModuleSize = 15, reassignThreshold
731 = 0, and mergeCutHeight = 0.25. Subnetwork eigengenes were extracted and termed "eigenpeptides".

732 One-sided fisher's exact tests were performed to assess the enrichment of Gene Ontology (GO)
733 Biological Processes, GO Cellular Compartments (R package "org.Mm.eg.db" version 3.15.0[82]), and
734 kinase substrates in each subnetwork relative to the entire phosphoproteome. Only pathways containing
735 three or more subnetwork phosphoproteins were tested. Kinase substrate enrichment was performed

using the same annotations as KSEA. P-values were adjusted within each analysis by the Benjamini-Hochberg procedure. Subnetwork phosphopeptides were mapped into insulin signalling temporal clusters defined in our previous study of insulin signalling dynamics[10], using PhosphositePlus Site Group IDs. The timepoint at which each cluster appeared to reach its maximum insulin-stimulated value was used as a measure of insulin response speed.

Glucose uptake correlations

For each insulin-regulated phosphopeptide, Pearson's correlation tests were performed to assess the linear association between ^{3}H-2DG uptake in insulin-stimulated mice and phosphopeptide insulin response values or unnormalized insulin-stimulated log2 intensity. Phosphopeptides were considered correlated with ^{3}H-2DG uptake when $q < 0.1$ and their Pearson's correlation coefficient was of substantial magnitude ($r > 0.35$ or $r < -0.35$). Pearson's correlation tests were also performed comparing insulin-stimulated ^{3}H-2DG uptake to KSEA enrichment scores in individual mice or using the median in each strain-diet combination.

Cell culture

GLUT4-HA-L6 myoblasts[83] were grown in α-MEM supplemented with 10% fetal bovine serum in a humidified chamber at 37 °C, 10% CO2. Differentiation was induced by changing media to α-MEM supplemented with 2% horse serum for 5 days.

Pfkfb3 overexpression

Platinum-E (Plat-E) retroviral packaging cells were grown to confluency and transfected with 10 µg total DNA: either pBabe puromycin empty vector, pBabe puromycin Pfkfb3 or pWZL neomycin HA-GLUT4. After 48 h retroviral media was collected and passed through a 0.45 µm filter. L6 myotubes were grown to confluence and retrovirally transfected with 2 mL of HA-GLUT4 neomycin viral media in the presence of 10 µg/ml polybrene. The following morning, cells were split into growth media containing neomycin (800 µg/ml) and passaged until only successfully transfected cells remained. These cells were then grown to confluence and retrovirally transfected again with 2 mL of either empty vector puromycin viral media or Pfkfb3 puromycin viral media in the presence of 10 µg/ml of polybrene. The following morning, cells were split into growth media containing both neomycin (800 µg/ml) and puromycin (2 µg/ml) and passaged until only successfully transfected cells remained in culture.

Extracellular acidification rate

The extracellular acidification rate (ECAR) of GLUT4-HA-L6 cells myotubes was measured using Seahorse XFp miniplates and a Seahorse XF HS Mini Analyzer (Seahorse Bioscience, Copenhagen, Denmark) as previously described[84]. Cells incubated in palmitate or BSA control were washed twice with Krebs-Ringer Bicarbonate Buffer (Sigma, K4002) and once with standard cell culture media

773 without bicarbonate (XF-DMEM, pH 7.4). Cells were then incubated in XF-DMEM without glucose
774 at 37°C for 1 h in a non-CO2 incubator, followed by assaying in the XFp Analyzer. ECAR was
775 measured after a 12-minute equilibration period followed by mix/wait/read cycles of 3/0/3 min. After
776 stabilizing the baseline rates, compounds were injected to reach a final concentration of: 10 mM
777 glucose, 5 µg/mL oligomycin, and 50 mM 2-deoxyglucose (2-DG), allowing estimation of glucose-
778 driven glycolysis (glucose ECAR - basal ECAR), glycolytic capacity (oligomycin ECAR - 2DG
779 ECAR), and non-glycolytic acidification (equal to 2DG ECAR). Data were normalized to protein
780 concentration and presented as a percentage of total ECAR.
781
782 ***2DG uptake in GLUT4-HA-L6 myotubes***
783 2-deoxyglucose (2DG) uptake into GLUT4-HA-L6 myotubes was performed as previously described
784 with modifications[83,85]. Cells were incubated overnight in αMEM supplemented with either BSA-
785 coupled 125 µM palmitic acid or BSA vehicle control before being washed 3x with 37 °C HEPES-
786 buffered saline (HBS). Cells were then incubated in HBS supplemented with 10 µM unlabelled 2-
787 deoxyglucose and either 0 or 100 nM insulin at 37°C for 15 min. Cells were then incubated for a further
788 5 min following the addition of 0.5 µCi/ml [^{3}H]-2-deoxyglucose in HBS. Cells were then washed on
789 ice 5x with ice-cold PBS and lysed in 1 M NaOH. For non-specific background uptake, 1 well per
790 condition was pre-treated with cytochalasin B. Counts were determined by Perkin Elmer Quantulus
791 GCT Liquid Scintillation Counter (Perkin Elmer, Waltham, MA, USA). 2DG uptake was expressed
792 relatively to protein concentration as determined by bicinchoninic acid (BCA) assay after neutralisation
793 with 1 M HCl and subtraction of non-specific uptake.
794
795 ***Immunoblotting***
796 GLUT4-HA-L6 myotubes were incubated overnight (16 h) in either BSA-conjugated 125 µM palmitate
797 or BSA vehicle control. Cells were optionally treated with insulin as described above, and then washed
798 in ice-cold PBS and lysed by scraping directly into 55 °C Laemmli sample buffer with 10 % (tris 2-
799 carboxyethyl phosphine; TCEP). Samples were sonicated for 24 s (3s on/3s off) and heated at 65 °C for
800 5 minutes. Samples were then resolved by SDS-PAGE as previously described[18], transferred onto PVDF
801 membranes and blocked in TBS-T (0.1% Tween in Tris-buffered saline) containing 5% skim milk for
802 1 h. Membranes were then washed 3 x 10 min in TBS-T and incubated overnight in primary antibodies
803 against Pfkfb3 (Proteintech Group; 13763-1-AP) and α-tubulin (Cell Signalling Technologies #2125;
804 diluted 1:1000). Insulin-stimulated cells were additionally incubated in primary antibodies against
805 pT308 Akt (Cell Signaling Technologies #2965; diluted 1:1000), pS473 Akt (Cell Signaling
806 Technologies #9271; diluted 1:1000), total pan-Akt (Cell Signaling Technologies #9272; diluted
807 1:1000), pS21/S9 GSK3α/β (Cell Signaling Technologies #9327; diluted 1:1000), pT246 PRAS40 (Cell
808 Signaling Technologies #13175; diluted 1:1000), total PRAS40 (Cell Signaling Technologies #2691,
809 diluted 1:1000, and 14-3-3 (Santa Cruz #sc-1657, diluted 1:5000). The following day membranes were

810 washed 3 x 10 min in TBS-T and incubated for 1 h in species-appropriate fluorescent antibodies.
811 Imaging and densitometry were performed using LI-COR Image Studio.

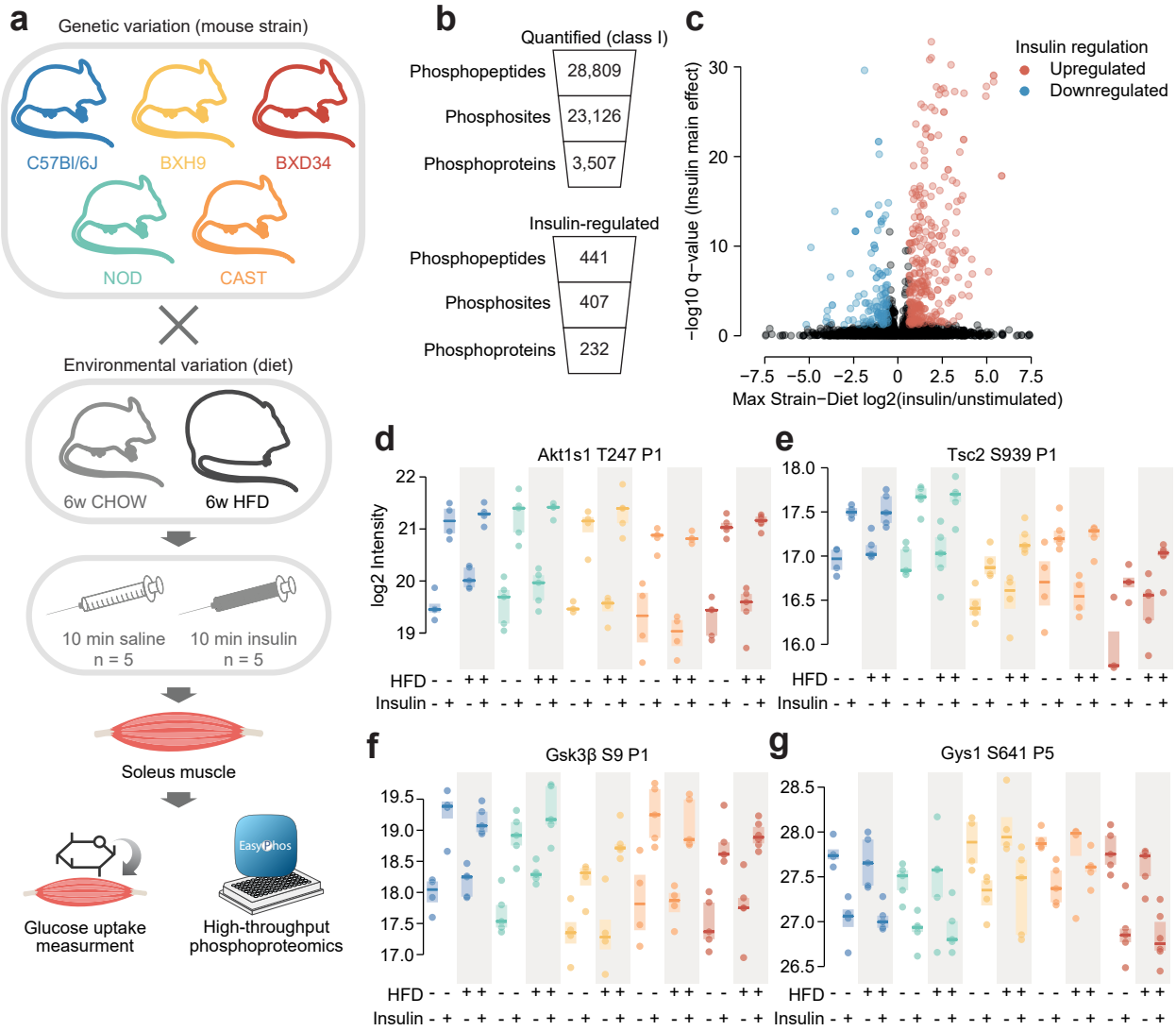

Figure 1: Phosphoproteomics of insulin signalling in mouse skeletal muscle. a) Workflow for skeletal muscle phosphoproteomics of insulin signalling. **b)** Quantification of skeletal muscle phosphoproteomics. **c)** Volcano plot identifying insulin-regulated phosphopeptides. The greatest log2(insulin/unstimulated) fold change across strain-diet combinations is plotted against significance (insulin stimulation main effect, three-way ANOVA). Three phosphopeptides with -log10 q-values greater than 35 were removed for visual clarity. **d-g)** Example insulin-regulated phosphopeptides. The protein and phosphorylated amino acid are indicated, as well as the number of phosphosites on the phosphopeptide (e.g. "P1"). n = 4-6 biological replicates.

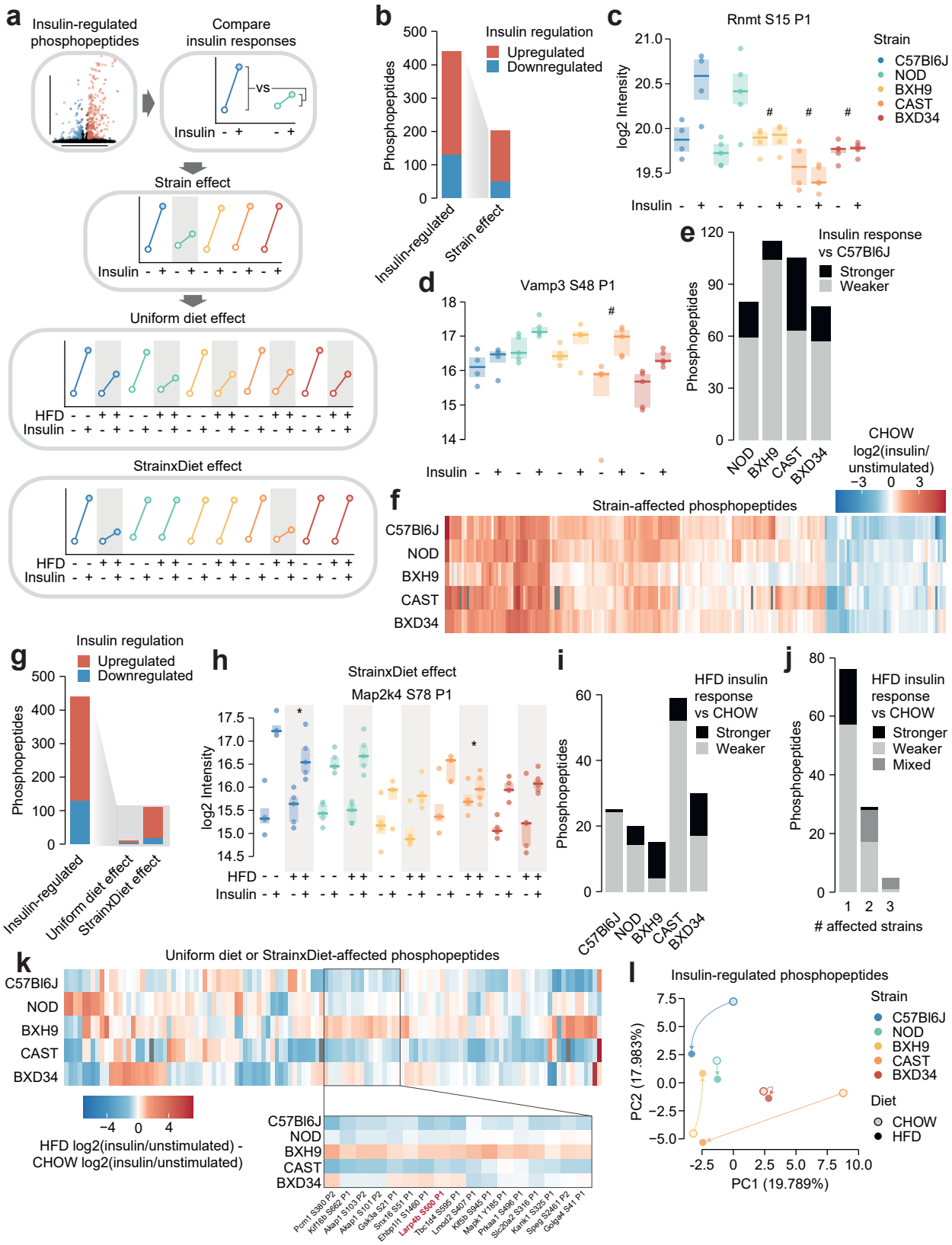

Figure 2: Genetics and diet modulate insulin signalling. a) Schematic for identifying effects of strain and diet on insulin signalling. **b)** The number of total insulin-regulated phosphopeptides and those with a Strain effect. **c-d)** Two phosphopeptides with Strain effects. ANOVAs were performed on CHOW insulin responses following two-sided t-tests comparing each strain to C57Bl6J (q-values: #). Only CHOW values are shown. **e)** The number of phosphopeptides with stronger or weaker insulin regulation in each strain compared to C57Bl6J. **f)** Heatmap displaying all insulin-regulated phosphopeptides with a Strain effect. Missing values are coloured

grey. **g)** The number of total insulin-regulated phosphopeptides and those with diet effects. **h)** A phosphopeptide with a StrainxDiet effect. A two-way ANOVA was performed on insulin response values followed by two-sided t-tests comparing HFD to CHOW within each strain (q-values: *). **i-j)** The number of phosphopeptides with a StrainxDiet effect in **i)** each strain, or **j)** each number of strains. Colour indicates whether the insulin response in HFD is stronger vs CHOW, weaker vs CHOW, or both in different strains ("Mixed"). **k)** Heatmap displaying all insulin-regulated phosphopeptides with a Uniform diet effect or StrainxDiet effect. Inset displays example sites where BXH9 effects contrasted other strains. **l)** PCA of all insulin-regulated phosphopeptides using the log2(insulin/unstimulated) fold changes for each Strain-Diet combination. The percentage of total variance explained by each principal component is indicated. */#: $0.01 \leq q < 0.05$, **/##: $0.001 \leq q < 0.01$, ***/###: $q < 0.001$. n = 4-6 biological replicates.

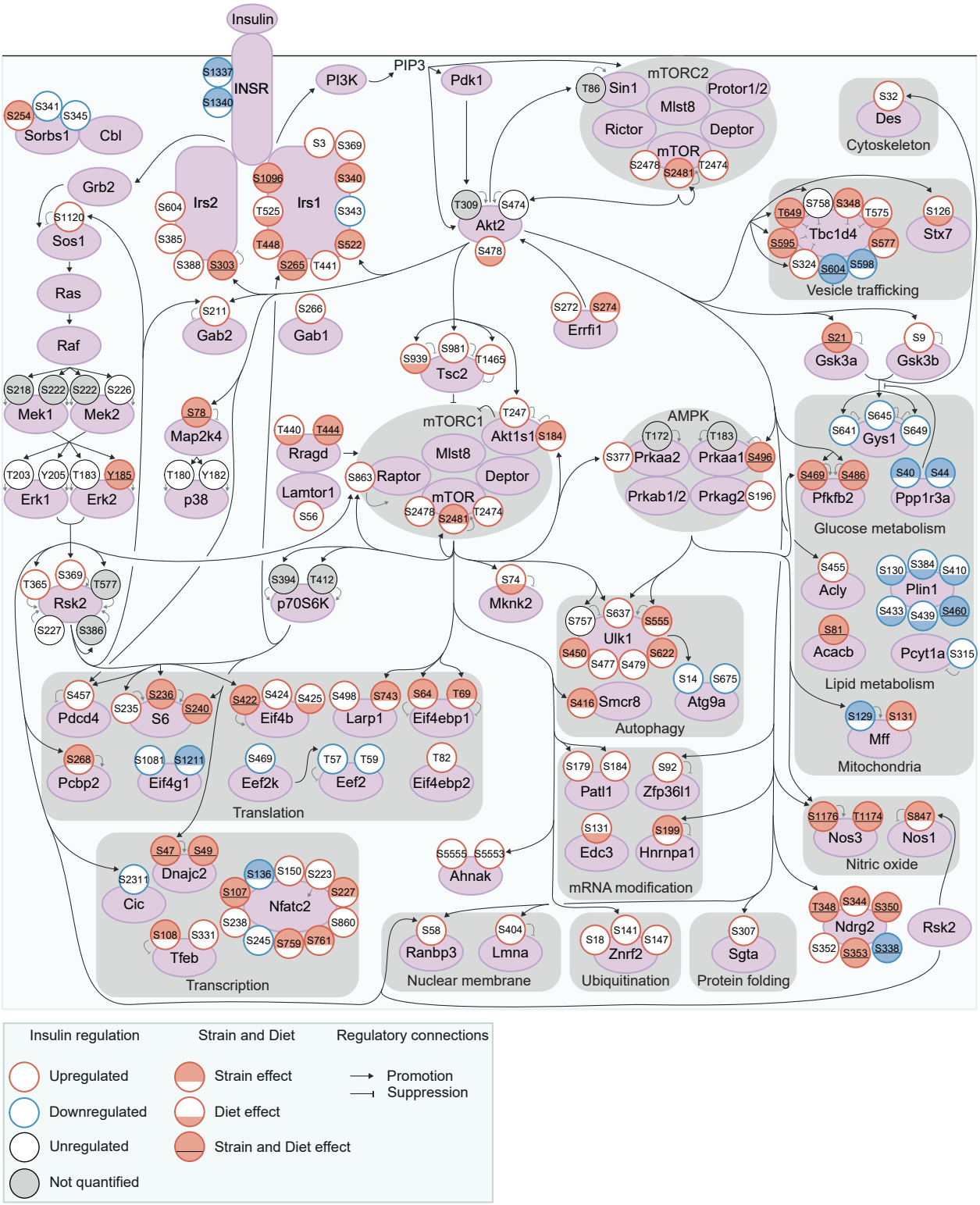

Figure 3: Exploring genetic and dietary modulation of the insulin signalling network. A curated network of 160 insulin-regulated phosphosites. Phosphosites are depicted as circles where the outline colour denotes the direction of insulin regulation, and the inner colour denotes the presence of Strain effects or Diet effects (either a StrainxDiet or Uniform diet effect). Black arrows indicate regulatory relationships from proteins to other proteins or phosphosites. Grey lines indicate phosphosite regulatory roles.

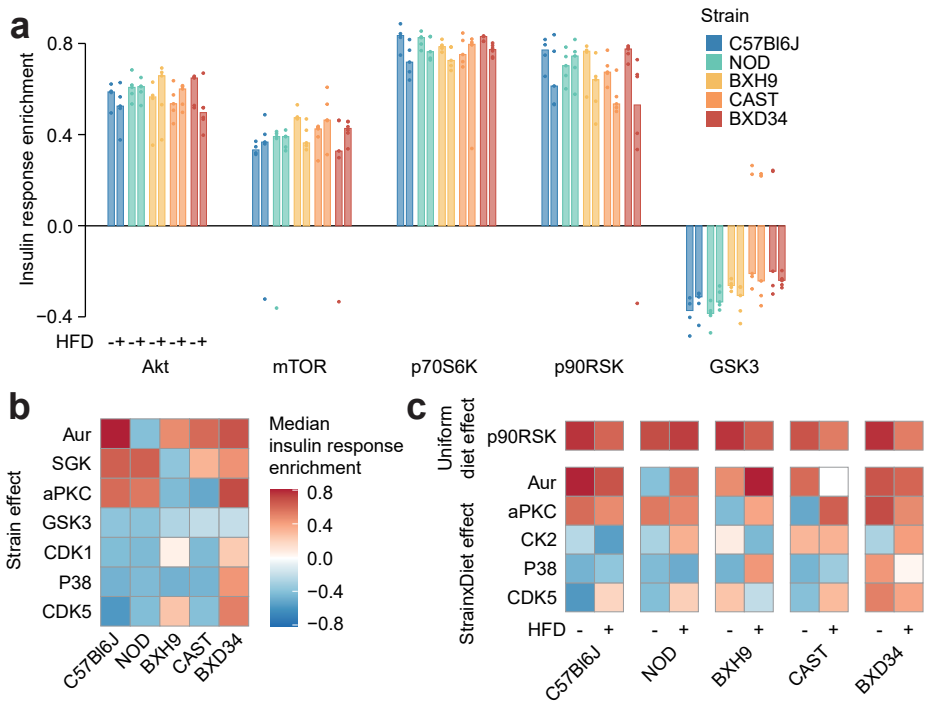

Figure 4: Genetics and diet rewire insulin-regulated kinase signalling. a) Kinase substrate enrichment analysis (KSEA)[37] of five canonical insulin-regulated kinases using insulin response values and kinase-substrate annotations from PhosphositePlus[32]. **b-c)** Kinase enrichment scores were tested for **b)** Strain effects (CHOW ANOVA adjusted $p < 0.05$) or **c)** StrainxDiet effects (two-way ANOVA interaction effect adjusted $p < 0.05$) and Uniform diet effects (Diet main effect adjusted $p < 0.05$, interaction effect adjusted $p \geq 0.05$). n = 4-6 biological replicates.

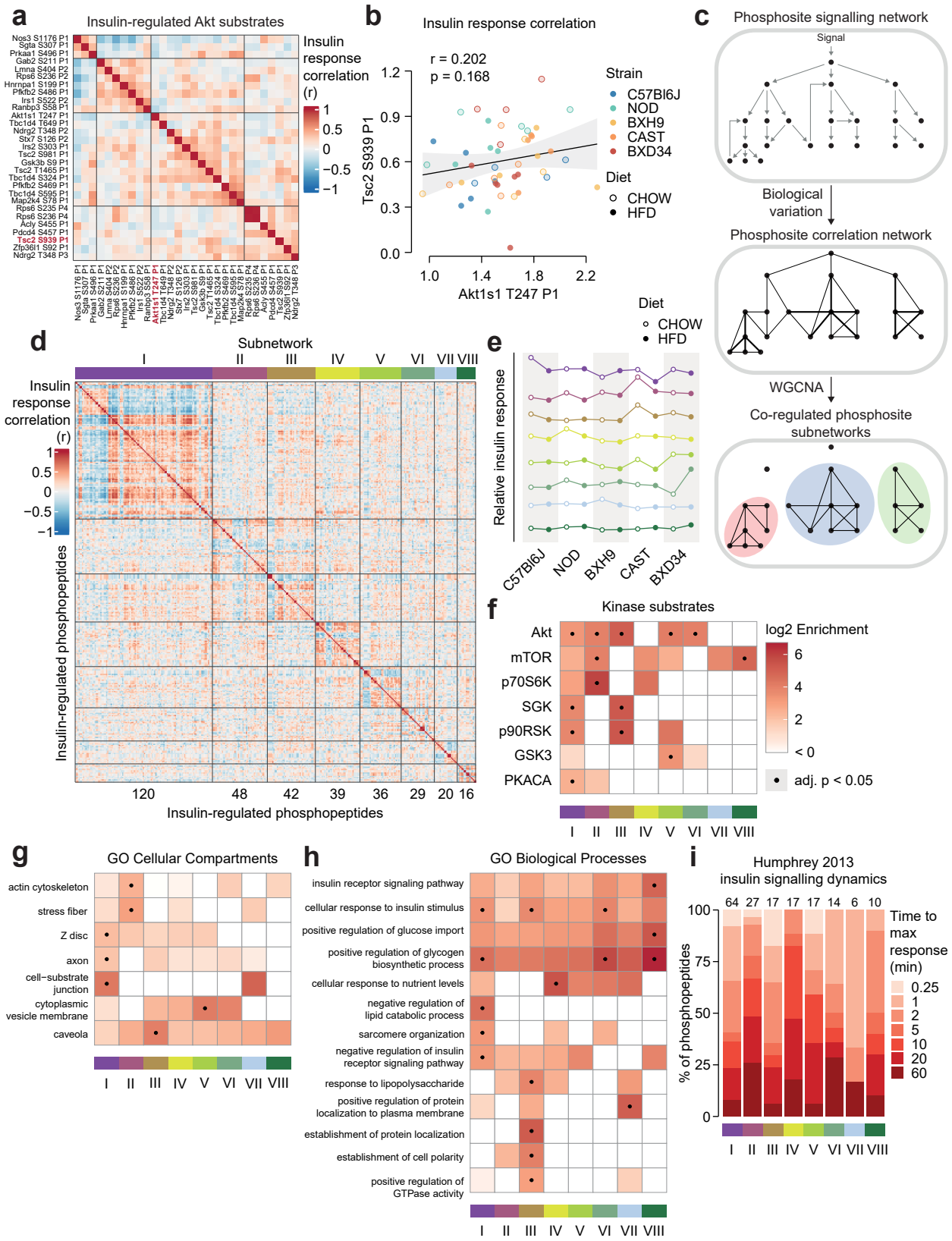

Figure 5: Biological variation reveals functional organisation of the insulin signalling network. **a)** Pairwise Pearson's correlation of the insulin response values of insulin-regulated Akt substrates. Substrates were separated into four clusters by hierarchical clustering followed by tree cutting. **b)** The correlation between insulin response values of the Akt substrates Tsc2 S939 and Akt1s1 T247. Linear regression is indicated with 95% confidence intervals. **c)** Rationale for performing WGCNA. **d)** Pairwise Pearson's correlation of all insulin-regulated phosphopeptides separated into WGCNA-derived subnetworks. The number of

phosphopeptides in each subnetwork is indicated below the heatmap. **e)** The "eigenpeptide" of each subnetwork. The median of each strain-diet combination is shown. **f-h)** The enrichment of **f)** PhosphositePlus-derived kinase-substrate annotations[32], **g)** GO cellular compartments, and **h)** GO biological processes within each subnetwork relative to the entire phosphoproteome (one-sided Fisher's exact test, Benjamini-Hochberg p-value adjustment). **i)** The time taken for phosphopeptides to reach maximum insulin-stimulated intensity in a previous study of insulin signalling dynamics[10]. The number of phosphopeptides mapped into the study is indicated above each bar.

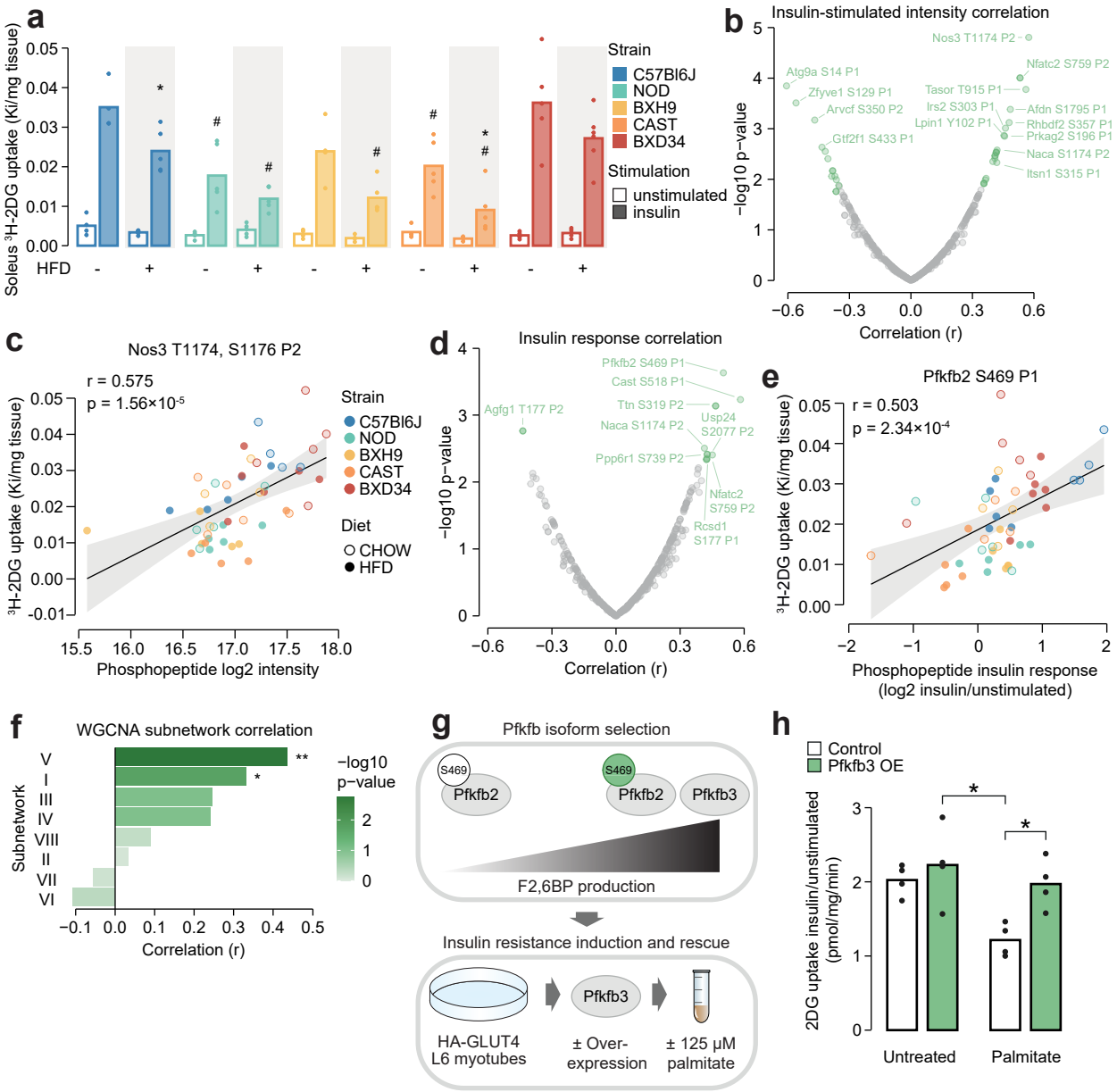

Figure 6: Leveraging biological variation to identify drivers of insulin responsiveness. a) The uptake of ^{3}H-2DG into mouse soleus muscle after a 10 min injection of insulin (1 U/kg lean mass; "insulin") or saline ("unstimulated") calculated as a rate constant (Ki). Two-sided t-tests were performed on insulin-stimulated uptake values to compare HFD to CHOW within each strain (adjusted p-value: *) or each strain to C57Bl6J within either diet (adjusted p-value: #). n = 4-6 biological replicates. **b)** Pearson's correlation between log2 intensity of insulin-regulated phosphopeptides and ^{3}H-2DG uptake within insulin-stimulated mice. Significantly correlated phosphopeptides (q-value < 0.1, r > 0.35 or r < -0.35) are coloured green and select correlated phosphopeptides are labelled. **c)** Correlation of Nos3 T1174, S1176 insulin-stimulated intensity with insulin-stimulated ^{3}H-2DG uptake. Linear regression is indicated with 95% confidence intervals. **d)** As in **b)**, using phosphopeptide insulin response values. **e)** Correlation of the Pfkfb2 S469 insulin response with insulin-stimulated ^{3}H-2DG uptake. **f)** Correlation of WGCNA subnetwork eigenpeptides with insulin-stimulated ^{3}H-2DG uptake. Significant correlations are indicated (*). **g)** Rationale and workflow for over-expressing Pfkfb3 to rescue palmitate-induced insulin resistance. **h)** The fold change of unstimulated to insulin-stimulated glucose uptake (100 nM insulin, 20 min) in L6-GLUT4-HA myotubes with or without Pfkfb3 overexpression, treated with palmitate (125 µM, 16 h) or BSA vehicle control. A two-way ANOVA was performed followed by

Tukey's posthoc tests (*). Not all significant comparisons are shown. n = 4 biological replicates. */#: $0.01 \leq p < 0.05$, **/##: $0.001 \leq p < 0.01$, ***/###: $p < 0.001$

References

1. Humphrey, S.J., James, D.E., and Mann, M. (2015). Protein Phosphorylation: A Major Switch Mechanism for Metabolic Regulation. Trends Endocrinol. Metab. *26*, 676–687.

2. Needham, E.J., Parker, B.L., Burykin, T., James, D.E., and Humphrey, S.J. (2019). Illuminating the dark phosphoproteome. Sci. Signal. *12*. 10.1126/scisignal.aau8645.

3. Olsen, J.V., Blagoev, B., Gnad, F., Macek, B., Kumar, C., Mortensen, P., and Mann, M. (2006). Global, in vivo, and site-specific phosphorylation dynamics in signaling networks. Cell *127*, 635–648.

4. Bodenmiller, B., Wanka, S., Kraft, C., Urban, J., Campbell, D., Pedrioli, P.G., Gerrits, B., Picotti, P., Lam, H., Vitek, O., Brusniak, M.-Y., Roschitzki, B., Zhang, C., Shokat, K.M., Schlapbach, R., Colman-Lerner, A., Nolan, G.P., Nesvizhskii, A.I., Peter, M., Loewith, R., von Mering, C., and Aebersold, R. (2010). Phosphoproteomic analysis reveals interconnected system-wide responses to perturbations of kinases and phosphatases in yeast. Sci. Signal. *3*, rs4.

5. Needham, E.J., Humphrey, S.J., Cooke, K.C., Fazakerley, D.J., Duan, X., Parker, B.L., and James, D.E. (2019). Phosphoproteomics of Acute Cell Stressors Targeting Exercise Signaling Networks Reveal Drug Interactions Regulating Protein Secretion. Cell Rep. *29*, 1524-1538.e6.

6. Leutert, M., Barente, A.S., Fukuda, N.K., Rodriguez-Mias, R.A., and Villén, J. (2022). The regulatory landscape of the yeast phosphoproteome. bioRxiv, 2022.10.23.513432. 10.1101/2022.10.23.513432.

7. Haeusler, R.A., McGraw, T.E., and Accili, D. (2018). Biochemical and cellular properties of insulin receptor signalling. Nat. Rev. Mol. Cell Biol. *19*, 31–44.

8. Gehart, H., Kumpf, S., Ittner, A., and Ricci, R. (2010). MAPK signalling in cellular metabolism: stress or wellness? EMBO Rep. *11*, 834–840.

9. Sylow, L., Jensen, T.E., Kleinert, M., Højlund, K., Kiens, B., Wojtaszewski, J., Prats, C., Schjerling, P., and Richter, E.A. (2013). Rac1 signaling is required for insulin-stimulated glucose uptake and is dysregulated in insulin-resistant murine and human skeletal muscle. Diabetes *62*, 1865–1875.

10. Humphrey, S.J., Yang, G., Yang, P., Fazakerley, D.J., Stöckli, J., Yang, J.Y., and James, D.E. (2013). Dynamic adipocyte phosphoproteome reveals that Akt directly regulates mTORC2. Cell Metab. *17*, 1009–1020.

11. Humphrey, S.J., Azimifar, S.B., and Mann, M. (2015). High-throughput phosphoproteomics reveals in vivo insulin signaling dynamics. Nat. Biotechnol. *33*, 990–995.

12. Krüger, M., Kratchmarova, I., Blagoev, B., Tseng, Y.-H., Kahn, C.R., and Mann, M. (2008). Dissection of the insulin signaling pathway via quantitative phosphoproteomics. Proc. Natl. Acad. Sci. U. S. A. *105*, 2451–2456.

13. James, D.E., Stöckli, J., and Birnbaum, M.J. (2021). The aetiology and molecular landscape of insulin resistance. Nat. Rev. Mol. Cell Biol. 10.1038/s41580-021-00390-6.

14. Fazakerley, D.J., Krycer, J.R., Kearney, A.L., Hocking, S.L., and James, D.E. (2019). Muscle and adipose tissue insulin resistance: malady without mechanism? J. Lipid Res. *60*, 1720–1732.

15. van Gerwen, J., Shun-Shion, A.S., and Fazakerley, D.J. (2023). Insulin signalling and GLUT4 trafficking in insulin resistance. Biochem. Soc. Trans. *51*, 1057–1069.

16. Hunter, D.J. (2005). Gene–environment interactions in human diseases. Nat. Rev. Genet. *6*, 287–298.

17. Civelek, M., and Lusis, A.J. (2014). Systems genetics approaches to understand complex traits. Nat. Rev. Genet. *15*, 34–48.

18. Nelson, M.E., Madsen, S., Cooke, K.C., Fritzen, A.M., Thorius, I.H., Masson, S.W.C., Carroll, L., Weiss, F.C., Seldin, M.M., Potter, M., Hocking, S.L., Fazakerley, D.J., Brandon, A.E., Thillainadesan, S., Senior, A.M., Cooney, G.J., Stöckli, J., and James, D.E. (2022). Systems-level analysis of insulin action in mouse strains provides insight into tissue- and pathway-specific interactions that drive insulin resistance. Cell Metab. *34*, 227-239.e6.

19. Montgomery, M.K., Hallahan, N.L., Brown, S.H., Liu, M., Mitchell, T.W., Cooney, G.J., and Turner, N. (2013). Mouse strain-dependent variation in obesity and glucose homeostasis in response to high-fat feeding. Diabetologia *56*, 1129–1139.

20. Grossbach, J., Gillet, L., Clément-Ziza, M., Schmalohr, C.L., Schubert, O.T., Schütter, M., Mawer, J.S.P., Barnes, C.A., Bludau, I., Weith, M., Tessarz, P., Graef, M., Aebersold, R., and Beyer, A. (2022). The impact of genomic variation on protein phosphorylation states and regulatory networks. Mol. Syst. Biol. *18*, e10712.

21. Zhang, T., Keele, G.R., Gyuricza, I.G., Vincent, M., Brunton, C., Bell, T.A., Hock, P., Shaw, G.D., Munger, S.C., de Villena, F.P.-M., Ferris, M.T., Paulo, J.A., Gygi, S.P., and Churchill, G.A. (2023). Multi-omics analysis identifies drivers of protein phosphorylation. Genome Biol. *24*, 52.

22. Needham, E.J., Hingst, J.R., Parker, B.L., Morrison, K.R., Yang, G., Onslev, J., Kristensen, J.M., Højlund, K., Ling, N.X.Y., Oakhill, J.S., Richter, E.A., Kiens, B., Petersen, J., Pehmøller, C., James, D.E., Wojtaszewski, J.F.P., and Humphrey, S.J. (2021). Personalized phosphoproteomics identifies functional signaling. Nat. Biotechnol. 10.1038/s41587-021-01099-9.

23. McCarthy, M.I., Abecasis, G.R., Cardon, L.R., Goldstein, D.B., Little, J., Ioannidis, J.P.A., and Hirschhorn, J.N. (2008). Genome-wide association studies for complex traits: consensus, uncertainty and challenges. Nat. Rev. Genet. *9*, 356–369.

24. Lusis, A.J., Seldin, M.M., Allayee, H., Bennett, B.J., Civelek, M., Davis, R.C., Eskin, E., Farber, C.R., Hui, S., Mehrabian, M., Norheim, F., Pan, C., Parks, B., Rau, C.D., Smith, D.J., Vallim, T., Wang, Y., and Wang, J. (2016). The Hybrid Mouse Diversity Panel: a resource for systems genetics analyses of metabolic and cardiovascular traits. J. Lipid Res. *57*, 925–942.

25. Burchfield, J.G., Kebede, M.A., Meoli, C.C., Stöckli, J., Tess Whitworth, P., Wright, A.L., Hoffman, N.J., Minard, A.Y., Ma, X., Krycer, J.R., Nelson, M.E., Tan, S.-X., Yau, B., Thomas, K.C., Wee, N.K.Y., Khor, E.-C., Enriquez, R.F., Vissel, B., Biden, T.J., Baldock, P.A., Hoehn, K.L., Cantley, J., Cooney, G.J., James, D.E., and Fazakerley, D.J. (2018). High dietary fat and sucrose result in an extensive and time-dependent deterioration in health of multiple physiological systems in mice. J. Biol. Chem. *293*, 5731–5745.

26. DeFronzo, R.A. (1988). The Triumvirate: β-Cell, Muscle, Liver: A Collusion Responsible for NIDDM. Diabetes *37*, 667–687.

27. Schiaffino, S., and Reggiani, C. (2011). Fiber types in mammalian skeletal muscles. Physiol. Rev. *91*, 1447–1531.

28. Humphrey, S.J., Karayel, O., James, D.E., and Mann, M. (2018). High-throughput and high-sensitivity phosphoproteomics with the EasyPhos platform. Nat. Protoc. *13*, 1897–1916.

29. Bekker-Jensen, D.B., Bernhardt, O.M., Hogrebe, A., Martinez-Val, A., Verbeke, L., Gandhi, T., Kelstrup, C.D., Reiter, L., and Olsen, J.V. (2020). Rapid and site-specific deep phosphoproteome

898 profiling by data-independent acquisition without the need for spectral libraries. Nat. Commun. *11*,
899 787.

900 30. Batista, T.M., Jayavelu, A.K., Wewer Albrechtsen, N.J., Iovino, S., Lebastchi, J., Pan, H., Dreyfuss,
901 J.M., Krook, A., Zierath, J.R., Mann, M., and Kahn, C.R. (2020). A Cell-Autonomous Signature
902 of Dysregulated Protein Phosphorylation Underlies Muscle Insulin Resistance in Type 2 Diabetes.
903 Cell Metab. *32*, 844-859.e5.

904 31. Haider, N., Lebastchi, J., Jayavelu, A.K., Batista, T.M., Pan, H., Dreyfuss, J.M., Carcamo-Orive,
905 I., Knowles, J.W., Mann, M., and Kahn, C.R. (2021). Signaling defects associated with insulin
906 resistance in non-diabetic and diabetic individuals and modification by sex. J. Clin. Invest.
907 10.1172/JCI151818.

908 32. Fazakerley, D.J., van Gerwen, J., Cooke, K.C., Duan, X., Needham, E.J., Díaz-Vegas, A., Madsen,
909 S., Norris, D.M., Shun-Shion, A.S., Krycer, J.R., Burchfield, J.G., Yang, P., Wade, M.R.,
910 Brozinick, J.T., James, D.E., and Humphrey, S.J. (2023). Phosphoproteomics reveals rewiring of
911 the insulin signaling network and multi-nodal defects in insulin resistance. Nat. Commun. *14*, 1–
912 20.

913 33. Hornbeck, P.V., Zhang, B., Murray, B., Kornhauser, J.M., Latham, V., and Skrzypek, E. (2015).
914 PhosphoSitePlus, 2014: mutations, PTMs and recalibrations. Nucleic Acids Res. *43*, D512-20.

915 34. Klip, A., McGraw, T.E., and James, D.E. (2019). Thirty sweet years of GLUT4. J. Biol. Chem.
916 *294*, 11369–11381.

917 35. Hoffman, N.J., Parker, B.L., Chaudhuri, R., Fisher-Wellman, K.H., Kleinert, M., Humphrey, S.J.,
918 Yang, P., Holliday, M., Trefely, S., Fazakerley, D.J., Stöckli, J., Burchfield, J.G., Jensen, T.E.,
919 Jothi, R., Kiens, B., Wojtaszewski, J.F.P., Richter, E.A., and James, D.E. (2015). Global
920 Phosphoproteomic Analysis of Human Skeletal Muscle Reveals a Network of Exercise-Regulated
921 Kinases and AMPK Substrates. Cell Metab. *22*, 922–935.

922 36. Ochoa, D., Jarnuczak, A.F., Viéitez, C., Gehre, M., Soucheray, M., Mateus, A., Kleefeldt, A.A.,
923 Hill, A., Garcia-Alonso, L., Stein, F., Krogan, N.J., Savitski, M.M., Swaney, D.L., Vizcaíno, J.A.,
924 Noh, K.-M., and Beltrao, P. (2020). The functional landscape of the human phosphoproteome. Nat.
925 Biotechnol. *38*, 365–373.

926 37. Schwenk, R.W., Angin, Y., Steinbusch, L.K.M., Dirkx, E., Hoebers, N., Coumans, W.A., Bonen,
927 A., Broers, J.L.V., van Eys, G.J., Glatz, J.F.C., and Others (2012). Overexpression of vesicle-
928 associated membrane protein (VAMP) 3, but not VAMP2, protects glucose transporter (GLUT) 4
929 protein translocation in an in vitro model of cardiac insulin resistance. J. Biol. Chem. *287*, 37530–
930 37539.

931 38. Barilari, M., Bonfils, G., Treins, C., Koka, V., De Villeneuve, D., Fabrega, S., and Pende, M.
932 (2017). ZRF1 is a novel S6 kinase substrate that drives the senescence programme. EMBO J. *36*,
933 736–750.

934 39. Agassandian, M., Zhou, J., Tephly, L.A., Ryan, A.J., Carter, A.B., and Mallampalli, R.K. (2005).
935 Oxysterols inhibit phosphatidylcholine synthesis via ERK docking and phosphorylation of
936 CTP:phosphocholine cytidylyltransferase. J. Biol. Chem. *280*, 21577–21587.

937 40. Hernandez-Armenta, C., Ochoa, D., Gonçalves, E., Saez-Rodriguez, J., and Beltrao, P. (2017).
938 Benchmarking substrate-based kinase activity inference using phosphoproteomic data.
939 Bioinformatics *33*, 1845–1851.

940 41. Tonks, K.T., Ng, Y., Miller, S., Coster, A.C.F., Samocha-Bonet, D., Iseli, T.J., Xu, A., Patrick, E.,
941 Yang, J.Y.H., Junutula, J.R., Modrusan, Z., Kolumam, G., Stöckli, J., Chisholm, D.J., James, D.E.,

and Greenfield, J.R. (2013). Impaired Akt phosphorylation in insulin-resistant human muscle is accompanied by selective and heterogeneous downstream defects. Diabetologia *56*, 875–885.

42. Zhang, B., and Horvath, S. (2005). A General Framework for Weighted Gene Co-Expression Network Analysis. Statistical Applications in Genetics and Molecular Biology *4*. 10.2202/1544-6115.1128.

43. Langfelder, P., and Horvath, S. (2008). WGCNA: an R package for weighted correlation network analysis. BMC Bioinformatics *9*, 559.

44. Roy, D., Perreault, M., and Marette, A. (1998). Insulin stimulation of glucose uptake in skeletal muscles and adipose tissues in vivo is NO dependent. Am. J. Physiol. *274*, E692-9.

45. Bahadoran, Z., Mirmiran, P., and Ghasemi, A. (2020). Role of Nitric Oxide in Insulin Secretion and Glucose Metabolism. Trends Endocrinol. Metab. *31*, 118–130.

46. Dimmeler, S., Fleming, I., Fisslthaler, B., Hermann, C., Busse, R., and Zeiher, A.M. (1999). Activation of nitric oxide synthase in endothelial cells by Akt-dependent phosphorylation. Nature *399*, 601–605.

47. Lundh, M., Petersen, P.S., Isidor, M.S., Kazoka-Sørensen, D.N., Plucińska, K., Shamsi, F., Ørskov, C., Tozzi, M., Brown, E.L., Andersen, E., Ma, T., Müller, U., Barrès, R., Kristiansen, V.B., Gerhart-Hines, Z., Tseng, Y.-H., and Emanuelli, B. (2019). Afadin is a scaffold protein repressing insulin action via HDAC6 in adipose tissue. EMBO Rep. *20*, e48216.

48. O'Neill, H.M. (2013). AMPK and Exercise: Glucose Uptake and Insulin Sensitivity. Diabetes Metab. J. *37*, 1–21.

49. Deprez, J., Vertommen, D., Alessi, D.R., Hue, L., and Rider, M.H. (1997). Phosphorylation and activation of heart 6-phosphofructo-2-kinase by protein kinase B and other protein kinases of the insulin signaling cascades. J. Biol. Chem. *272*, 17269–17275.

50. Marsin, A.-S., Bertrand, L., Rider, M.H., Deprez, J., Beauloye, C., Vincent, M.F., Van den Berghe, G., Carling, D., and Hue, L. (2000). Phosphorylation and activation of heart PFK-2 by AMPK has a role in the stimulation of glycolysis during ischaemia. Curr. Biol. *10*, 1247–1255.

51. Ros, S., and Schulze, A. (2013). Balancing glycolytic flux: the role of 6-phosphofructo-2-kinase/fructose 2,6-bisphosphatases in cancer metabolism. Cancer Metab *1*, 8.

52. Stöckli, J., Fazakerley, D.J., and James, D.E. (2011). GLUT4 exocytosis. J. Cell Sci. *124*, 4147–4159.

53. Dokken, B.B., Sloniger, J.A., and Henriksen, E.J. (2005). Acute selective glycogen synthase kinase-3 inhibition enhances insulin signaling in prediabetic insulin-resistant rat skeletal muscle. Am. J. Physiol. Endocrinol. Metab. *288*, E1188-94.

54. Henriksen, E.J., and Teachey, M.K. (2007). Short-term in vitro inhibition of glycogen synthase kinase 3 potentiates insulin signaling in type I skeletal muscle of Zucker Diabetic Fatty rats. Metabolism *56*, 931–938.

55. Ring, D.B., Johnson, K.W., Henriksen, E.J., Nuss, J.M., Goff, D., Kinnick, T.R., Ma, S.T., Reeder, J.W., Samuels, I., Slabiak, T., Wagman, A.S., Hammond, M.-E.W., and Harrison, S.D. (2003). Selective glycogen synthase kinase 3 inhibitors potentiate insulin activation of glucose transport and utilization in vitro and in vivo. Diabetes *52*, 588–595.

56. Masson, S.W.C., Madsen, S., Cooke, K.C., Potter, M., Vegas, A.D., Carroll, L., Thillainadesan, S., Cutler, H.B., Walder, K.R., Cooney, G.J., Morahan, G., Stöckli, J., and James, D.E. (2023).

Leveraging genetic diversity to identify small molecules that reverse mouse skeletal muscle insulin resistance. Elife *12*. 10.7554/eLife.86961.

57. Trefely, S., Khoo, P.-S., Krycer, J.R., Chaudhuri, R., Fazakerley, D.J., Parker, B.L., Sultani, G., Lee, J., Stephan, J.-P., Torres, E., Jung, K., Kuijl, C., James, D.E., Junutula, J.R., and Stöckli, J. (2015). Kinome Screen Identifies PFKFB3 and Glucose Metabolism as Important Regulators of the Insulin/Insulin-like Growth Factor (IGF)-1 Signaling Pathway. J. Biol. Chem. *290*, 25834–25846.

58. Dephoure, N., Gould, K.L., Gygi, S.P., and Kellogg, D.R. (2013). Mapping and analysis of phosphorylation sites: a quick guide for cell biologists. Mol. Biol. Cell *24*, 535–542.

59. Hoehn, K.L., Salmon, A.B., Hohnen-Behrens, C., Turner, N., Hoy, A.J., Maghzal, G.J., Stocker, R., Van Remmen, H., Kraegen, E.W., Cooney, G.J., Richardson, A.R., and James, D.E. (2009). Insulin resistance is a cellular antioxidant defense mechanism. Proc. Natl. Acad. Sci. U. S. A. *106*, 17787–17792.

60. Tortorella, L.L., and Pilch, P.F. (2002). C2C12 myocytes lack an insulin-responsive vesicular compartment despite dexamethasone-induced GLUT4 expression. Am. J. Physiol. Endocrinol. Metab. *283*, E514-24.

61. Portiér, G.L., Benders, A.G., Oosterhof, A., Veerkamp, J.H., and van Kuppevelt, T.H. (1999). Differentiation markers of mouse C2C12 and rat L6 myogenic cell lines and the effect of the differentiation medium. In Vitro Cell. Dev. Biol. Anim. *35*, 219–227.

62. Bloom, J., and Cross, F.R. (2007). Multiple levels of cyclin specificity in cell-cycle control. Nat. Rev. Mol. Cell Biol. *8*, 149–160.

63. Steinberg, G.R., and Hardie, D.G. (2023). New insights into activation and function of the AMPK. Nat. Rev. Mol. Cell Biol. *24*, 255–272.

64. Lavoie, H., Gagnon, J., and Therrien, M. (2020). ERK signalling: a master regulator of cell behaviour, life and fate. Nat. Rev. Mol. Cell Biol. *21*, 607–632.

65. Meyuhas, O. (2015). Ribosomal Protein S6 Phosphorylation: Four Decades of Research. Int. Rev. Cell Mol. Biol. *320*, 41–73.

66. Johnson, J.L., Yaron, T.M., Huntsman, E.M., Kerelsky, A., Song, J., Regev, A., Lin, T.-Y., Liberatore, K., Cizin, D.M., Cohen, B.M., Vasan, N., Ma, Y., Krismer, K., Robles, J.T., van de Kooij, B., van Vlimmeren, A.E., Andrée-Busch, N., Käufer, N.F., Dorovkov, M.V., Ryazanov, A.G., Takagi, Y., Kastenhuber, E.R., Goncalves, M.D., Hopkins, B.D., Elemento, O., Taatjes, D.J., Maucuer, A., Yamashita, A., Degterev, A., Uduman, M., Lu, J., Landry, S.D., Zhang, B., Cossentino, I., Linding, R., Blenis, J., Hornbeck, P.V., Turk, B.E., Yaffe, M.B., and Cantley, L.C. (2023). An atlas of substrate specificities for the human serine/threonine kinome. Nature *613*, 759–766.

67. Chen, J., Spracklen, C.N., Marenne, G., Varshney, A., Corbin, L.J., Luan, J., Willems, S.M., Wu, Y., Zhang, X., Horikoshi, M., Boutin, T.S., Mägi, R., Waage, J., Li-Gao, R., Chan, K.H.K., Yao, J., Anasanti, M.D., Chu, A.Y., Claringbould, A., Heikkinen, J., Hong, J., Hottenga, J.-J., Huo, S., Kaakinen, M.A., Louie, T., März, W., Moreno-Macias, H., Ndungu, A., Nelson, S.C., Nolte, I.M., North, K.E., Raulerson, C.K., Ray, D., Rohde, R., Rybin, D., Schurmann, C., Sim, X., Southam, L., Stewart, I.D., Wang, C.A., Wang, Y., Wu, P., Zhang, W., Ahluwalia, T.S., Appel, E.V.R., Bielak, L.F., Brody, J.A., Burtt, N.P., Cabrera, C.P., Cade, B.E., Chai, J.F., Chai, X., Chang, L.-C., Chen, C.-H., Chen, B.H., Chitrala, K.N., Chiu, Y.-F., de Haan, H.G., Delgado, G.E., Demirkan, A., Duan, Q., Engmann, J., Fatumo, S.A., Gayán, J., Giulianini, F., Gong, J.H., Gustafsson, S., Hai, Y., Hartwig, F.P., He, J., Heianza, Y., Huang, T., Huerta-Chagoya, A., Hwang, M.Y., Jensen, R.A., Kawaguchi, T., Kentistou, K.A., Kim, Y.J., Kleber, M.E., Kooner, I.K., Lai, S., Lange, L.A.,

Langefeld, C.D., Lauzon, M., Li, M., Ligthart, S., Liu, J., Loh, M., Long, J., Lyssenko, V., Mangino, M., Marzi, C., Montasser, M.E., Nag, A., Nakatochi, M., Noce, D., Noordam, R., Pistis, G., Preuss, M., Raffield, L., Rasmussen-Torvik, L.J., Rich, S.S., Robertson, N.R., Rueedi, R., Ryan, K., Sanna, S., Saxena, R., Schraut, K.E., Sennblad, B., Setoh, K., Smith, A.V., Sparsø, T., Strawbridge, R.J., Takeuchi, F., Tan, J., Trompet, S., van den Akker, E., van der Most, P.J., Verweij, N., Vogel, M., Wang, H., Wang, C., Wang, N., Warren, H.R., Wen, W., Wilsgaard, T., Wong, A., Wood, A.R., Xie, T., Zafarmand, M.H., Zhao, J.-H., Zhao, W., Amin, N., Arzumanyan, Z., Astrup, A., Bakker, S.J.L., Baldassarre, D., Beekman, M., Bergman, R.N., Bertoni, A., Blüher, M., Bonnycastle, L.L., Bornstein, S.R., Bowden, D.W., Cai, Q., Campbell, A., Campbell, H., Chang, Y.C., de Geus, E.J.C., Dehghan, A., Du, S., Eiriksdottir, G., Farmaki, A.E., Frånberg, M., Fuchsberger, C., Gao, Y., Gjesing, A.P., Goel, A., Han, S., Hartman, C.A., Herder, C., Hicks, A.A., Hsieh, C.-H., Hsueh, W.A., Ichihara, S., Igase, M., Ikram, M.A., Johnson, W.C., Jørgensen, M.E., Joshi, P.K., Kalyani, R.R., Kandeel, F.R., Katsuya, T., Khor, C.C., Kiess, W., Kolcic, I., Kuulasmaa, T., Kuusisto, J., Läll, K., Lam, K., Lawlor, D.A., Lee, N.R., Lemaitre, R.N., Li, H., Lifelines Cohort Study, Lin, S.-Y., Lindström, J., Linneberg, A., Liu, J., Lorenzo, C., Matsubara, T., Matsuda, F., Mingrone, G., Mooijaart, S., Moon, S., Nabika, T., Nadkarni, G.N., Nadler, J.L., Nelis, M., Neville, M.J., Norris, J.M., Ohyagi, Y., Peters, A., Peyser, P.A., Polasek, O., Qi, Q., Raven, D., Reilly, D.F., Reiner, A., Rivideneira, F., Roll, K., Rudan, I., Sabanayagam, C., Sandow, K., Sattar, N., Schürmann, A., Shi, J., Stringham, H.M., Taylor, K.D., Teslovich, T.M., Thuesen, B., Timmers, P.R.H.J., Tremoli, E., Tsai, M.Y., Uitterlinden, A., van Dam, R.M., van Heemst, D., van Hylckama Vlieg, A., van Vliet-Ostaptchouk, J.V., Vangipurapu, J., Vestergaard, H., Wang, T., Willems van Dijk, K., Zemunik, T., Abecasis, G.R., Adair, L.S., Aguilar-Salinas, C.A., Alarcón-Riquelme, M.E., An, P., Aviles-Santa, L., Becker, D.M., Beilin, L.J., Bergmann, S., Bisgaard, H., Black, C., Boehnke, M., Boerwinkle, E., Böhm, B.O., Bønnelykke, K., Boomsma, D.I., Bottinger, E.P., Buchanan, T.A., Canouil, M., Caulfield, M.J., Chambers, J.C., Chasman, D.I., Chen, Y.-D.I., Cheng, C.-Y., Collins, F.S., Correa, A., Cucca, F., de Silva, H.J., Dedoussis, G., Elmståhl, S., Evans, M.K., Ferrannini, E., Ferrucci, L., Florez, J.C., Franks, P.W., Frayling, T.M., Froguel, P., Gigante, B., Goodarzi, M.O., Gordon-Larsen, P., Grallert, H., Grarup, N., Grimsgaard, S., Groop, L., Gudnason, V., Guo, X., Hamsten, A., Hansen, T., Hayward, C., Heckbert, S.R., Horta, B.L., Huang, W., Ingelsson, E., James, P.S., Jarvelin, M.-R., Jonas, J.B., Jukema, J.W., Kaleebu, P., Kaplan, R., Kardia, S.L.R., Kato, N., Keinanen-Kiukaanniemi, S.M., Kim, B.-J., Kivimaki, M., Koistinen, H.A., Kooner, J.S., Körner, A., Kovacs, P., Kuh, D., Kumari, M., Kutalik, Z., Laakso, M., Lakka, T.A., Launer, L.J., Leander, K., Li, H., Lin, X., Lind, L., Lindgren, C., Liu, S., Loos, R.J.F., Magnusson, P.K.E., Mahajan, A., Metspalu, A., Mook-Kanamori, D.O., Mori, T.A., Munroe, P.B., Njølstad, I., O'Connell, J.R., Oldehinkel, A.J., Ong, K.K., Padmanabhan, S., Palmer, C.N.A., Palmer, N.D., Pedersen, O., Pennell, C.E., Porteous, D.J., Pramstaller, P.P., Province, M.A., Psaty, B.M., Qi, L., Raffel, L.J., Rauramaa, R., Redline, S., Ridker, P.M., Rosendaal, F.R., Saaristo, T.E., Sandhu, M., Saramies, J., Schneiderman, N., Schwarz, P., Scott, L.J., Selvin, E., Sever, P., Shu, X.-O., Slagboom, P.E., Small, K.S., Smith, B.H., Snieder, H., Sofer, T., Sørensen, T.I.A., Spector, T.D., Stanton, A., Steves, C.J., Stumvoll, M., Sun, L., Tabara, Y., Tai, E.S., Timpson, N.J., Tönjes, A., Tuomilehto, J., Tusie, T., Uusitupa, M., van der Harst, P., van Duijn, C., Vitart, V., Vollenweider, P., Vrijkotte, T.G.M., Wagenknecht, L.E., Walker, M., Wang, Y.X., Wareham, N.J., Watanabe, R.M., Watkins, H., Wei, W.B., Wickremasinghe, A.R., Willemsen, G., Wilson, J.F., Wong, T.-Y., Wu, J.-Y., Xiang, A.H., Yanek, L.R., Yengo, L., Yokota, M., Zeggini, E., Zheng, W., Zonderman, A.B., Rotter, J.I., Gloyn, A.L., McCarthy, M.I., Dupuis, J., Meigs, J.B., Scott, R.A., Prokopenko, I., Leong, A., Liu, C.-T., Parker, S.C.J., Mohlke, K.L., Langenberg, C., Wheeler, E., Morris, A.P., Barroso, I., and Meta-Analysis of Glucose and Insulin-related Traits Consortium (MAGIC) (2021). The trans-ancestral genomic architecture of glycemic traits. Nat. Genet. *53*, 840–860.

68. Molendijk, J., Blazev, R., Mills, R.J., Ng, Y.-K., Watt, K.I., Chau, D., Gregorevic, P., Crouch, P.J., Hilton, J.B.W., Lisowski, L., Zhang, P., Reue, K., Lusis, A.J., Hudson, J.E., James, D.E., Seldin, M.M., and Parker, B.L. (2022). Proteome-wide systems genetics identifies UFMylation as a regulator of skeletal muscle function. Elife *11*. 10.7554/eLife.82951.

1083 69. Attwood, M.M., Fabbro, D., Sokolov, A.V., Knapp, S., and Schiöth, H.B. (2021). Trends in kinase
1084 drug discovery: targets, indications and inhibitor design. Nat. Rev. Drug Discov. *20*, 839–861.

1085 70. Eduati, F., Jaaks, P., Wappler, J., Cramer, T., Merten, C.A., Garnett, M.J., and Saez-Rodriguez, J.
1086 (2020). Patient-specific logic models of signaling pathways from screenings on cancer biopsies to
1087 prioritize personalized combination therapies. Mol. Syst. Biol. *16*, e8664.

1088 71. Montagud, A., Béal, J., Tobalina, L., Traynard, P., Subramanian, V., Szalai, B., Alföldi, R., Puskás,
1089 L., Valencia, A., Barillot, E., Saez-Rodriguez, J., and Calzone, L. (2022). Patient-specific Boolean
1090 models of signalling networks guide personalised treatments. Elife *11*. 10.7554/eLife.72626.

1091 72. Houstis, N., Rosen, E.D., and Lander, E.S. (2006). Reactive oxygen species have a causal role in
1092 multiple forms of insulin resistance. Nature *440*, 944–948.

1093 73. Fazakerley, D.J., Minard, A.Y., Krycer, J.R., Thomas, K.C., Stöckli, J., Harney, D.J., Burchfield,
1094 J.G., Maghzal, G.J., Caldwell, S.T., Hartley, R.C., Stocker, R., Murphy, M.P., and James, D.E.
1095 (2018). Mitochondrial oxidative stress causes insulin resistance without disrupting oxidative
1096 phosphorylation. J. Biol. Chem. *293*, 7315–7328.

1097 74. Su, Z., Burchfield, J.G., Yang, P., Humphrey, S.J., Yang, G., Francis, D., Yasmin, S., Shin, S.-Y.,
1098 Norris, D.M., Kearney, A.L., Astore, M.A., Scavuzzo, J., Fisher-Wellman, K.H., Wang, Q.-P.,
1099 Parker, B.L., Neely, G.G., Vafaee, F., Chiu, J., Yeo, R., Hogg, P.J., Fazakerley, D.J., Nguyen, L.K.,
1100 Kuyucak, S., and James, D.E. (2019). Global redox proteome and phosphoproteome analysis
1101 reveals redox switch in Akt. Nat. Commun. *10*, 5486.

1102 75. Piazza, I., Kochanowski, K., Cappelletti, V., Fuhrer, T., Noor, E., Sauer, U., and Picotti, P. (2018).
1103 A Map of Protein-Metabolite Interactions Reveals Principles of Chemical Communication. Cell
1104 *172*, 358-372.e23.

1105 76. Hicks, K.G., Cluntun, A.A., Schubert, H.L., Hackett, S.R., Berg, J.A., Leonard, P.G., Ajalla Aleixo,
1106 M.A., Zhou, Y., Bott, A.J., Salvatore, S.R., Chang, F., Blevins, A., Barta, P., Tilley, S., Leifer, A.,
1107 Guzman, A., Arok, A., Fogarty, S., Winter, J.M., Ahn, H.-C., Allen, K.N., Block, S., Cardoso, I.A.,
1108 Ding, J., Dreveny, I., Gasper, W.C., Ho, Q., Matsuura, A., Palladino, M.J., Prajapati, S., Sun, P.,
1109 Tittmann, K., Tolan, D.R., Unterlass, J., VanDemark, A.P., Vander Heiden, M.G., Webb, B.A.,
1110 Yun, C.-H., Zhao, P., Wang, B., Schopfer, F.J., Hill, C.P., Nonato, M.C., Muller, F.L., Cox, J.E.,
1111 and Rutter, J. (2023). Protein-metabolite interactomics of carbohydrate metabolism reveal
1112 regulation of lactate dehydrogenase. Science *379*, 996–1003.

1113 77. Sano, H., Kane, S., Sano, E., Mîinea, C.P., Asara, J.M., Lane, W.S., Garner, C.W., and Lienhard,
1114 G.E. (2003). Insulin-stimulated phosphorylation of a Rab GTPase-activating protein regulates
1115 GLUT4 translocation. J. Biol. Chem. *278*, 14599–14602.

1116 78. Parks, B.W., Sallam, T., Mehrabian, M., Psychogios, N., Hui, S.T., Norheim, F., Castellani, L.W.,
1117 Rau, C.D., Pan, C., Phun, J., Zhou, Z., Yang, W.-P., Neuhaus, I., Gargalovic, P.S., Kirchgessner,
1118 T.G., Graham, M., Lee, R., Tontonoz, P., Gerszten, R.E., Hevener, A.L., and Lusis, A.J. (2015).
1119 Genetic architecture of insulin resistance in the mouse. Cell Metab. *21*, 334–347.

1120 79. Yardeni, T., Eckhaus, M., Morris, H.D., Huizing, M., and Hoogstraten-Miller, S. (2011). Retro-
1121 orbital injections in mice. Lab Anim. *40*, 155–160.

1122 80. Goodner, C.J., Hom, F.G., and Berrie, M.A. (1980). Investigation of the effect of insulin upon
1123 regional brain glucose metabolism in the rat in vivo. Endocrinology *107*, 1827–1832.

1124 81. Storey, J.D. (2002). A direct approach to false discovery rates. J. R. Stat. Soc. Series B Stat.
1125 Methodol. *64*, 479–498.

1126 82. Carlson, M. (2019). org. Mm. eg. db: Genome wide annotation for Mouse. R package version 3.2.
1127 3. Bioconductor. London, United Kingdom: Genome Biology (BMC).

1128 83. Carey, A.L., Steinberg, G.R., Macaulay, S.L., Thomas, W.G., Holmes, A.G., Ramm, G., Prelovsek,
1129 O., Hohnen-Behrens, C., Watt, M.J., James, D.E., Kemp, B.E., Pedersen, B.K., and Febbraio, M.A.
1130 (2006). Interleukin-6 increases insulin-stimulated glucose disposal in humans and glucose uptake
1131 and fatty acid oxidation in vitro via AMP-activated protein kinase. Diabetes *55*, 2688–2697.

1132 84. Krycer, J.R., Elkington, S.D., Diaz-Vegas, A., Cooke, K.C., Burchfield, J.G., Fisher-Wellman,
1133 K.H., Cooney, G.J., Fazakerley, D.J., and James, D.E. (2020). Mitochondrial oxidants, but not
1134 respiration, are sensitive to glucose in adipocytes. J. Biol. Chem. *295*, 99–110.

1135 85. Masson, S.W.C., Woodhead, J.S.T., D'Souza, R.F., Broome, S.C., MacRae, C., Cho, H.C., Atiola,
1136 R.D., Futi, T., Dent, J.R., Shepherd, P.R., and Merry, T.L. (2021). β-Catenin is required for optimal
1137 exercise- and contraction-stimulated skeletal muscle glucose uptake. J. Physiol. *599*, 3897–3912.

1138

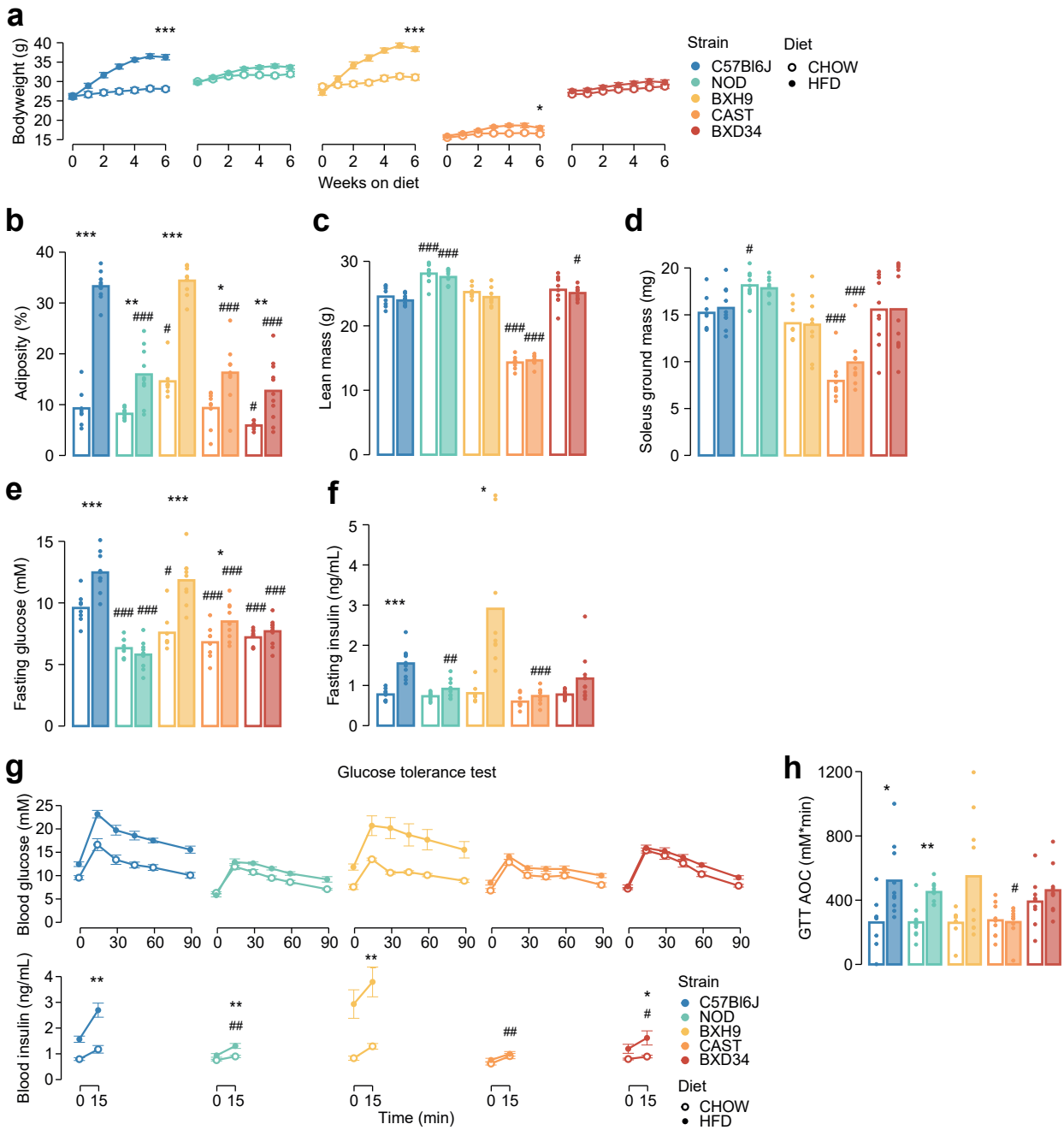

Figure S1: Genetics and diet alter morphometric and metabolic phenotypes. Related to Fig. 1. **a)** Mouse bodyweight was measured during a six-week diet regimen. Two-sided t-tests were performed to compare HFD to CHOW within each strain after six weeks, following Benjamini-Hochberg p-value adjustment (*). **b-d)** Measurement of **b)** adiposity, **c)** lean mass, **d)** ground soleus mass, **e)** fasting blood glucose, and **f)** fasting blood insulin at the end of the diet regimen. **g)** At the end of the diet regimen a glucose tolerance test was performed. **h)** The area of the blood glucose curve (GTT AOC) was calculated. In **b-h)**, two-sided t-tests were performed to compare HFD to CHOW within each strain (*) or to compare each strain to C57Bl6J within either diet (#). P-values were adjusted by the Benjamini-Hochberg procedure. Error bars indicate SEM. In **g)** t-tests were only performed on 15-minute blood insulin levels. No comparisons across strains on CHOW were significant. n = 8-11 biological replicates. */#: $0.01 \leq p < 0.05$, **/##: $0.001 \leq p < 0.01$, ***/###: $p < 0.001$

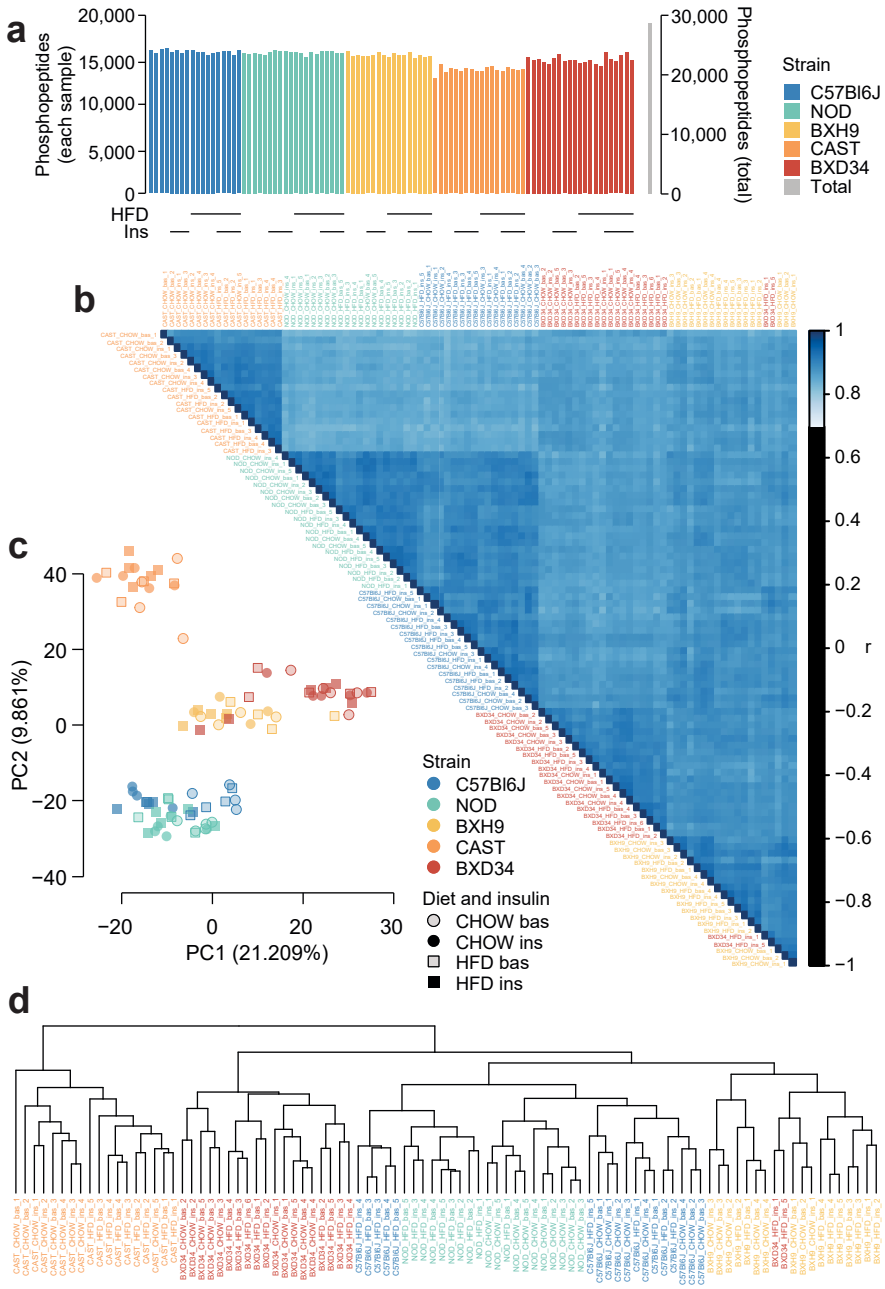

Figure S2: Quality control analysis of phosphoproteomics data. Related to Fig. 1. **a)** The number of unique class I phosphopeptides quantified in each sample and in total. **b)** Pearson's correlation was performed between each pair of samples. Samples are ordered by hierarchical clustering. **c)** Principal component analysis was performed on the phosphoproteome. The first two principal components (PC1 and PC2) are plotted for each sample and the percentage of overall variance explained by each principal component is indicated. "bas": unstimulated, "ins": insulin-stimulated. **d)** Hierarchical clustering was performed on all samples.

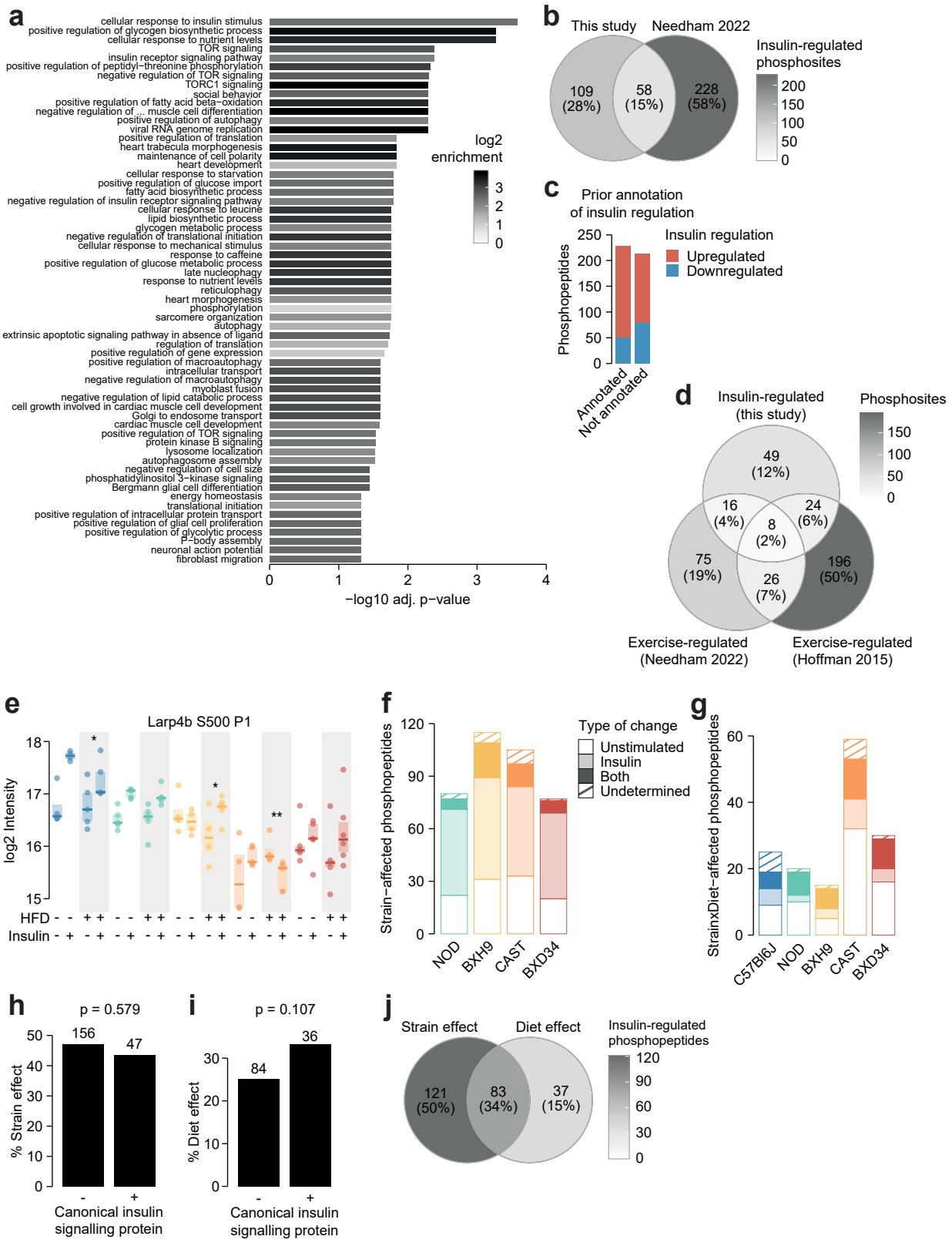

Figure S3: Characterisation of the insulin-regulated phosphoproteome. Related to Fig. 1-3. **a)** The enrichment of GO biological processes in genes containing insulin-regulated phosphopeptides relative to the entire phosphoproteome (one-sided Fisher's exact test, Benjamini-Hochberg p-value adjustment). Only significant pathways are shown (adj. $p < 0.05$). The pathway "negative regulation of vascular associated smooth muscle cell differentiation" is abbreviated. **b)** The number of phosphosites regulated by insulin in this study or a previous phosphoproteomic study of human skeletal muscle[1]. Only phosphosites quantified in both

studies were considered. **c)** The number of insulin-regulated phosphopeptides with prior annotation of insulin regulation in the PhosphositePlus database[2]. **d)** The number of phosphosites regulated by insulin this study or regulated by exercise in two human phosphoproteomics studies[1,3]. Only phosphosites quantified in all three studies were considered. **e)** A phosphopeptide where HFD-feeding enhanced insulin responses in BXH9 but suppressed insulin responses in C57Bl6J and CAST. A two-way ANOVA was performed on insulin response values followed by two-sided t-tests comparing HFD to CHOW within each strain (q-values: *). **f)** Phosphopeptides with a Strain effect were examined to determine whether the effect was due to altered unstimulated phosphorylation ("Unstimulated"; Strain/C57Bl6J fold change > 1.3 in unstimulated samples), altered insulin-stimulated phosphorylation ("Insulin"; Strain/C57Bl6J fold change > 1.3 in insulin-stimulated samples), or both ("Both"). A proportion of phosphopeptides passed neither of these filters ("Undetermined"). **g)** The same analysis was performed on StrainxDiet-affected phosphopeptides, using the HFD/CHOW fold changes in either unstimulated or insulin-stimulated samples for each strain. **h-i)** The percentage of **h)** Strain effects and **i)** Diet effects (Uniform diet or StrainxDiet effect) among canonical or noncanonical insulin signalling proteins. P-values indicate two-sided Fisher's exact tests. The number of phosphopeptides in each group is shown. **j)** The overlap of Strain and Diet effects.

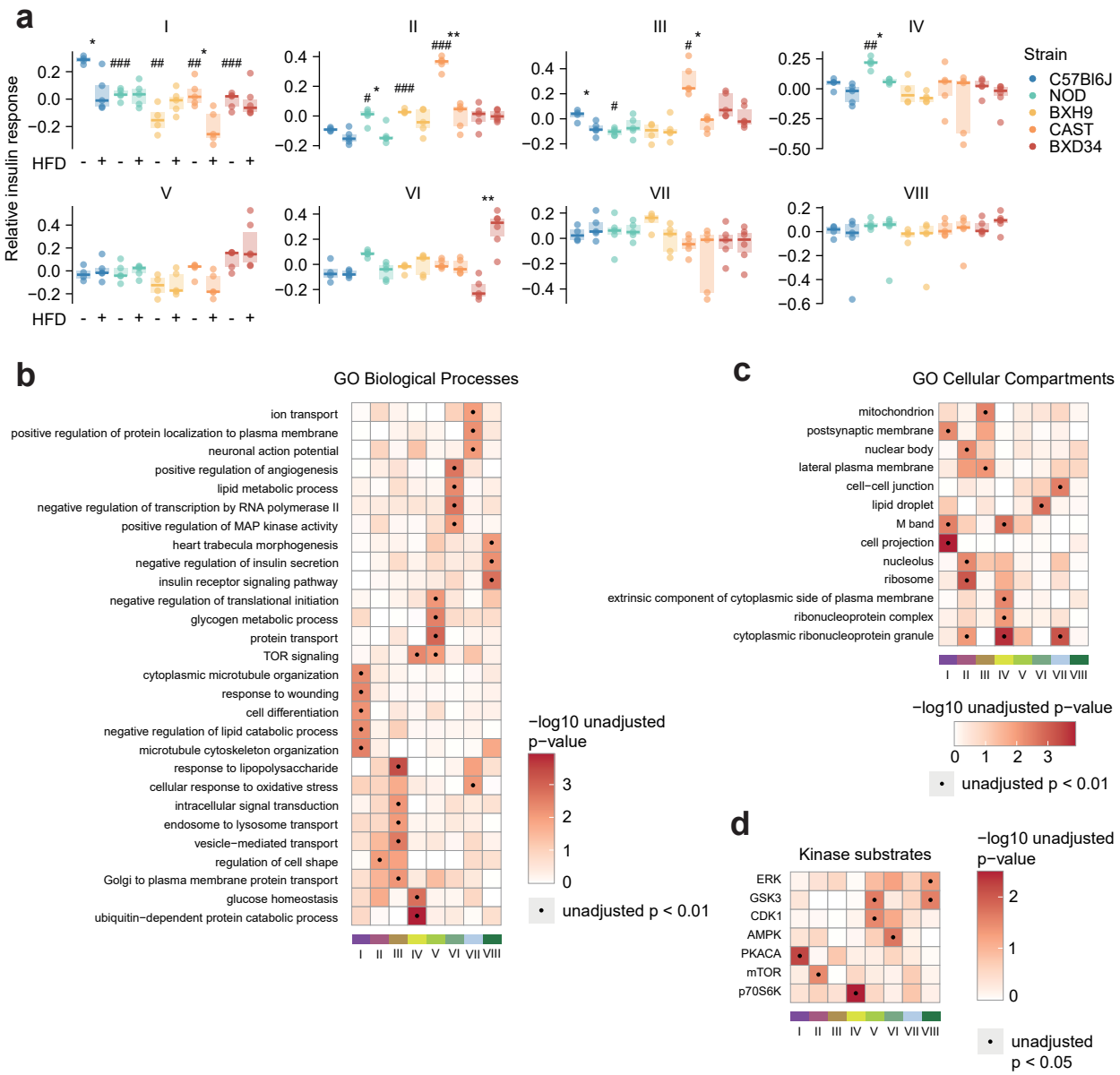

Figure S4: Characterising insulin signalling subnetworks. Related to Fig. 5. **a)** The eigenpeptides of each WGCNA-derived subnetwork. ANOVAs were performed on CHOW values following two-sided t-tests comparing each strain to C57Bl6J (Benjamini-Hochberg-adjusted p-values: #), and two-way ANOVAs were performed on all values followed by two-sided t-tests comparing HFD to CHOW within each strain (adjusted p-values: *). **b-d)** Rank-based enrichment of GO biological pathways, GO cellular compartments, and PhosphositePlus kinase substrates using phosphopeptide module membership scores with the "geneSetTest" function from the R package "limma". Membership score is defined as the absolute Pearson's correlation coefficient between a phosphopeptide's insulin response and the subnetwork's eigenpeptide. */#: $0.01 \leq p < 0.05$, **/##: $0.001 \leq p < 0.01$, ***/###: $p < 0.001$

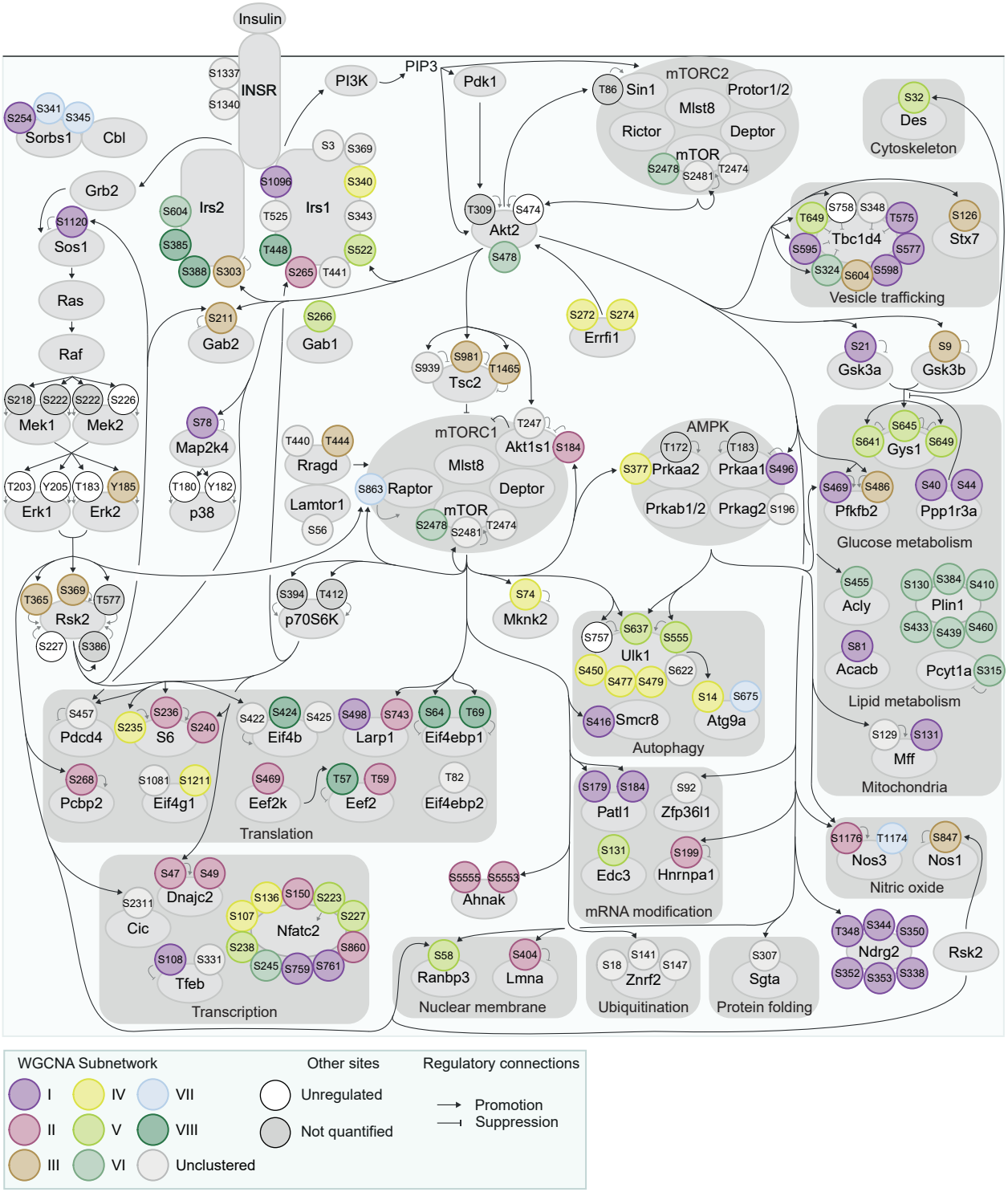

Figure S5: Organisation of insulin signalling subnetworks. Related to Fig. 5. The curated insulin signalling network displayed in Fig. 3 was annotated with WGCNA subnetworks from Fig. 5.

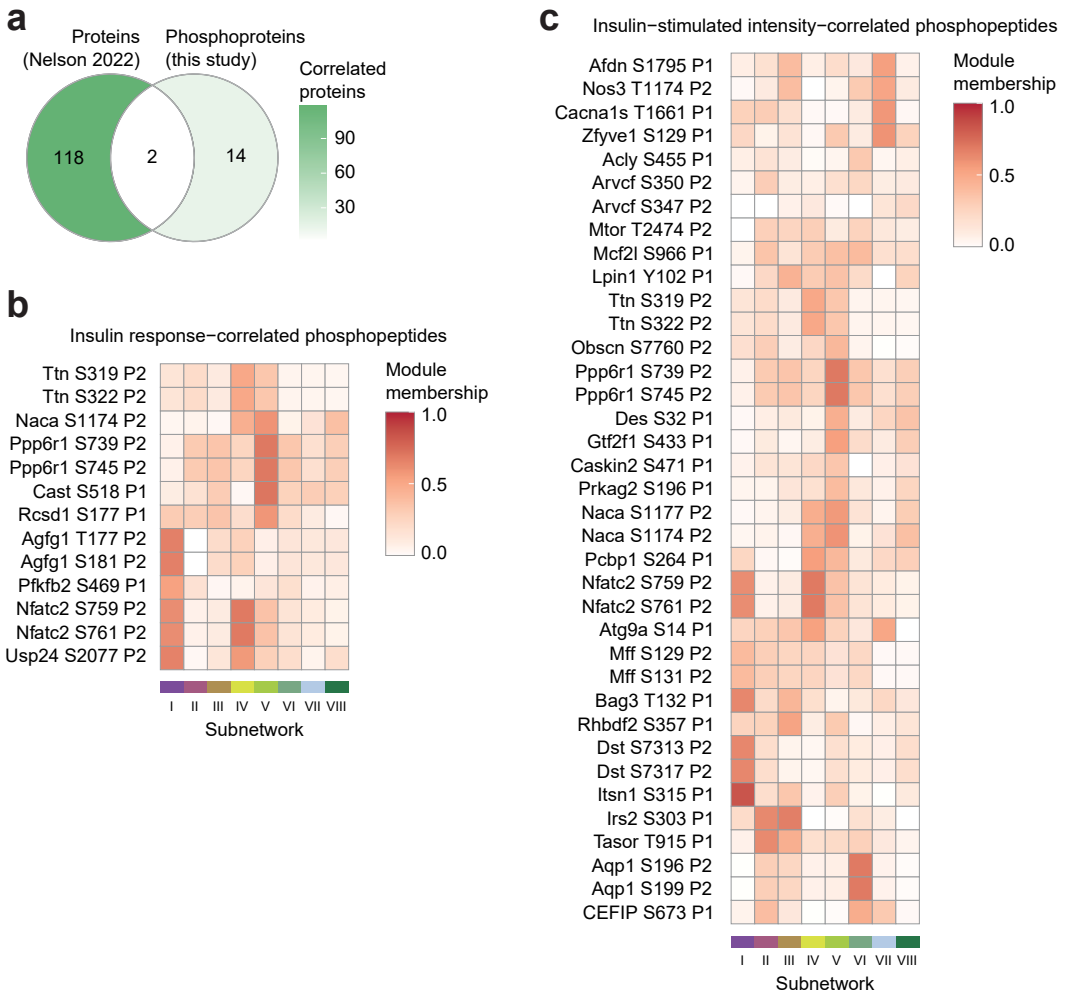

Figure S6: Characterisation of glucose-uptake correlated phosphosites. Related to Fig. 6. **a)** The intersection of proteins correlated with insulin-stimulated glucose uptake in the soleus of seven inbred mouse strains fed CHOW or HFD[4] ($p < 0.1$, $r > 0.35$ or < -0.35), with proteins containing glucose-uptake correlated phosphopeptides in this study. Only (phospho)proteins quantified in both studies are shown. **b-c)** The subnetwork membership scores for glucose-uptake correlated phosphopeptides using **b)** insulin-stimulated phosphopeptide intensity, or **c)** phosphopeptide insulin response values. Membership score is defined as the absolute Pearson's correlation coefficient between a phosphopeptide's insulin response and the subnetwork's eigenpeptide.

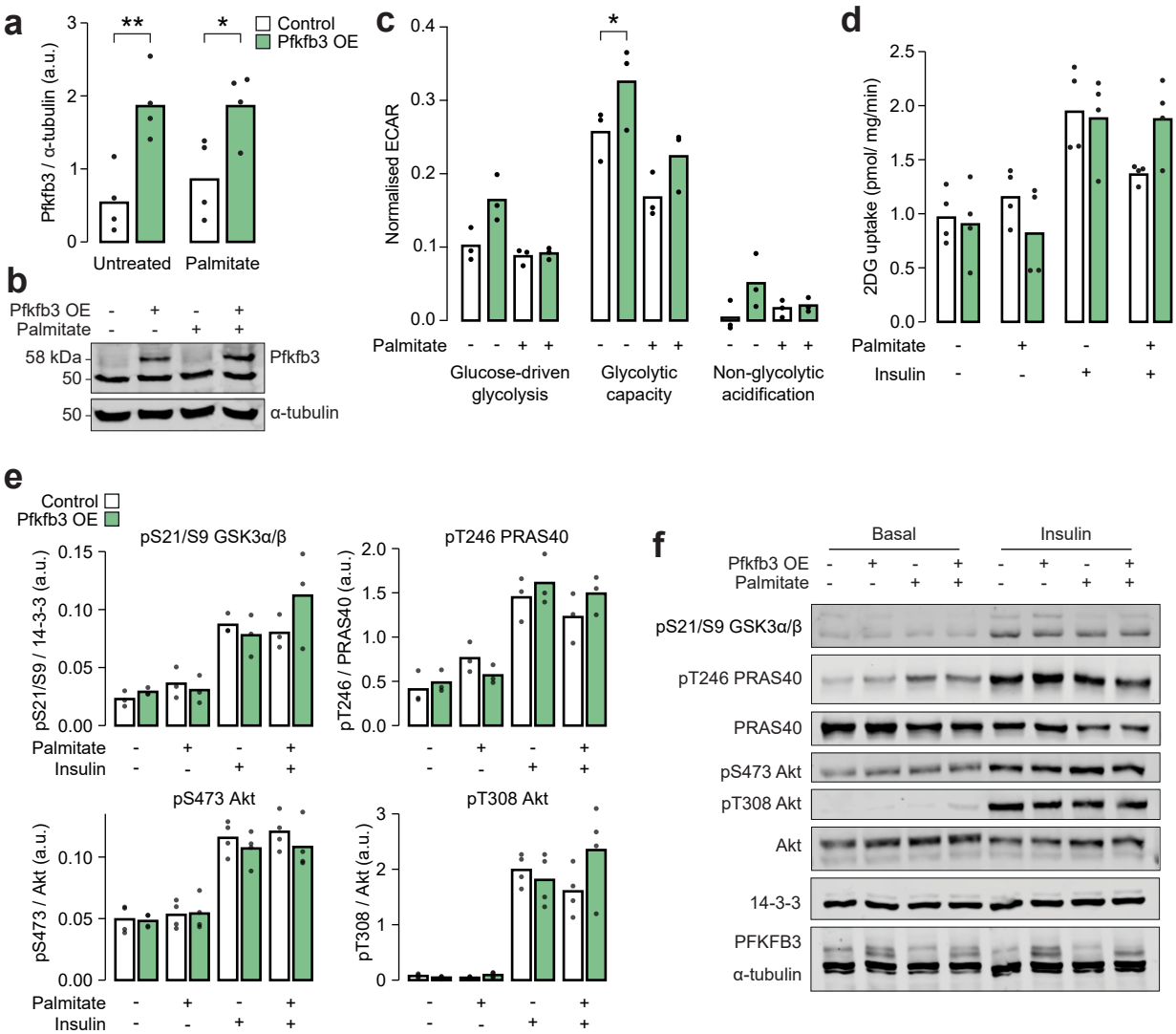

Figure S7: Overexpression of Pfkfb3 enhances glycolytic capacity and reverses palmitate-induced insulin resistance. Related to Fig. 6. **a)** Quantification and **b)** representative blot for immunoblotting of Pfkfb3 in L6-GLUT4-HA myotubes with or without Pfkfb3 overexpression, treated with palmitate (125 µM, 16 h) or BSA vehicle control. Two-way ANOVA was performed followed by Šidák's post-hoc tests assessing the effect of Pfkfb3 overexpression (*). n = 4 biological replicates. **c)** Extracellular acidification rate (ECAR) in L6-GLUT4-HA myotubes treated with glucose (10 mM, "Glucose-driven glycolysis"), oligomycin (5 µg/mL, "Glycolytic capacity"), or 2-deoxyglucose (50mM, "Non-glycolytic acidification"). A two-way ANOVA was performed followed by Tukey's posthoc tests comparing conditions within each of the three treatments (*). Not all significant comparisons are shown. n = 3 biological replicates. **d)** Unstimulated and insulin-stimulated glucose uptake (100 nM insulin, 20 min) in L6-GLUT4-HA myotubes. Insulin/unstimulated fold changes are shown in **Fig. 6h**. **e)** Quantification and **f)** representative blot for immunoblotting of insulin signalling phosphosites in unstimulated or insulin-stimulated (100 nM, 20 min) L6-GLUT4-HA myotubes.

*/#: $0.01 \leq p < 0.05$, **/##: $0.001 \leq p < 0.01$, ***/###: $p < 0.001$

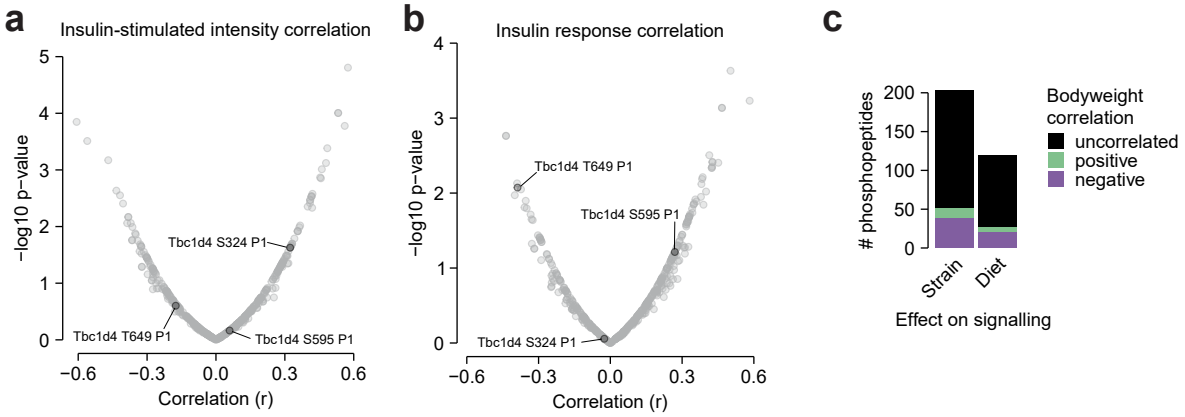

Figure S8: Additional glucose uptake correlation analysis. Related to Discussion. **a-b)** The correlation of insulin-stimulated glucose uptake with insulin-regulated phosphopeptides using **a)** insulin-stimulated phosphopeptide intensity, or **b)** phosphopeptide insulin response values, as displayed in **Fig. 6**. Canonical regulatory phosphosites on Tbc1d4 are indicated. The fourth canonical regulatory site S758 was not analysed due to insufficient quantification (quantified in 4/94 samples). **c)** The correlation of mouse bodyweight with the insulin responses of Strain or Diet-affected phosphopeptides either in CHOW-fed mice (Strain effects) or across both diets (Diet effects). The number of positively correlated (Pearson's correlation, $q < 0.1$, $r > 0.35$) and negatively correlated ($q < 0.1$, $r < -0.35$) phosphopeptides is shown.

Table S1: Muscle phosphoproteomics

(Page 1 "01_quantification") Normalized LFQ intensities of class I phosphopeptides. (Page 2 "02_analysis") Statistical analysis of phosphoproteome data.

Table S2: Overlap between insulin and exercise-regulated phosphosites

Insulin-regulated phosphosites from this study that were additionally regulated by exercise either in Needham et al.[1] or Hoffman et al.[3].

Phosphosite details				*Exercise regulation*	
PhosphositePlus					
Site Group ID	**Gene**	**Uniprot**	**Phosphosite**	**Hoffman 2015**	**Needham 2022**
450254	Eef2	P58252	T59	+	+
448040	Eef2	P58252	T57	+	+
470754	Mff	Q6PCP5	S131	+	+
470753	Mff	Q6PCP5	S129	+	+
453632	Larp1	Q6ZQ58	S498	+	+
455925	Tbc1d4	Q8BYJ6	S324	+	+
4762876	Svil	Q8K4L3	S300	+	+
448238	Gys1	Q9Z1E4	S645	+	+
480145	Tns1	E9Q0S6	S1054	+	
3176152	Ulk1	O70405	S450	+	
448064	Rps6ka3	P18654	S369	+	
469782	Dnajc2	P54103	S47	+	
486522	Pcbp1	P60335	S264	+	
448094	Rps6	P62754	S240	+	
448093	Rps6	P62754	S236	+	
447594	Mapk1	P63085	Y185	+	
453577	Patl1	Q3TC46	S179	+	
447527	Eif4ebp1	Q60876	S64	+	
482918	Pcbp2	Q61990	S268	+	
4731870	Speg	Q62407	S542	+	
14570198	Atg9a	Q68FE2	S675	+	
455922	Tbc1d4	Q8BYJ6	S348	+	
471364	Lpin1	Q91ZP3	S923	+	
448239	Gys1	Q9Z1E4	S649	+	
4693547	Ttn	A2ASS6	S322		+
480195	Usp24	B1AY13	S1296		+
10782556	Usp24	B1AY13	S1282		+
483808	Akap13	E9Q394	S2692		+
3208338	Akap1	O08715	S103		+
3831732	Tom1	O88746	S376		+
2048085	Rab12	P35283	S20		+
447655	Map2k4	P47809	S78		+
4720237	Lmod2	Q3UHZ5	T391		+
450706	Hspb6	Q5EBG6	S16		+
4726016	Tom1l2	Q5SRX1	S394		+
4716961	Slc20a2	Q80UP8	S316		+
17544627	Lmod1	Q8BVA4	S511		+
11180047	Tbc1d4	Q8BYJ6	S604		+
455921	Tbc1d4	Q8BYJ6	T649		+
3195560	Golga4	Q91VW5	S41		+
485723	Plekhf2	Q91WB4	S226		+
4772204	Ehbp1l1	Q99MS7	S1460		+
470067	Akt1s1	Q9D1F4	T247		+
452430	Plec	Q9QXS1	S4620		+

451009	Ndrg2	Q9QYG0	T348	+
468257	Ndrg2	Q9QYG0	S338	+
468259	Ndrg2	Q9QYG0	S344	+
447886	Nos1	Q9Z0J4	S847	+

Table S3: Insulin signalling subnetworks

WGCNA-derived subnetworks of insulin-regulated phosphopeptides.

Table S4: Association of kinase enrichment with insulin-stimulated glucose uptake

Pearson's correlation of KSEA enrichment scores with insulin-stimulated glucose uptake for all kinases with Strain or Diet effects. Correlation was performed on all values or on the medians of each Strain-Diet combination.

	Correlating all values		***Correlating Strain-Diet medians***	
Kinase	**r**	**p**	**r**	**p**
SGK	0.026282557	0.85773407	-0.114513813	0.752760165
Aur	0.181856398	0.221176679	0.446186208	0.196168185
p90RSK	0.042637179	0.771137201	0.392619919	0.261741297
aPKC	0.020857899	0.886881337	0.059269839	0.870801728
GSK3	-0.023496391	0.872683503	0.200939915	0.577765996
CDK5	0.092355979	0.527940053	0.136553891	0.706796386
P38	0.186315084	0.199914602	0.202333014	0.575075383
CDK1	0.134654975	0.356287427	0.245970422	0.493328434
CK2	0.062152944	0.671383691	-0.206449396	0.567152858

Supplementary references

1. Needham, E.J., Hingst, J.R., Parker, B.L., Morrison, K.R., Yang, G., Onslev, J., Kristensen, J.M., Højlund, K., Ling, N.X.Y., Oakhill, J.S., Richter, E.A., Kiens, B., Petersen, J., Pehmøller, C., James, D.E., Wojtaszewski, J.F.P., and Humphrey, S.J. (2021). Personalized phosphoproteomics identifies functional signaling. Nat. Biotechnol. 10.1038/s41587-021-01099-9.
2. Hornbeck, P.V., Zhang, B., Murray, B., Kornhauser, J.M., Latham, V., and Skrzypek, E. (2015). PhosphoSitePlus, 2014: mutations, PTMs and recalibrations. Nucleic Acids Res. *43*, D512-20.
3. Hoffman, N.J., Parker, B.L., Chaudhuri, R., Fisher-Wellman, K.H., Kleinert, M., Humphrey, S.J., Yang, P., Holliday, M., Trefely, S., Fazakerley, D.J., Stöckli, J., Burchfield, J.G., Jensen, T.E., Jothi, R., Kiens, B., Wojtaszewski, J.F.P., Richter, E.A., and James, D.E. (2015). Global Phosphoproteomic Analysis of Human Skeletal Muscle Reveals a Network of Exercise-Regulated Kinases and AMPK Substrates. Cell Metab. *22*, 922–935.
4. Nelson, M.E., Madsen, S., Cooke, K.C., Fritzen, A.M., Thorius, I.H., Masson, S.W.C., Carroll, L., Weiss, F.C., Seldin, M.M., Potter, M., Hocking, S.L., Fazakerley, D.J., Brandon, A.E., Thillainadesan, S., Senior, A.M., Cooney, G.J., Stöckli, J., and James, D.E. (2022). Systems-level analysis of insulin action in mouse strains provides insight into tissue- and pathway-specific interactions that drive insulin resistance. Cell Metab. *34*, 227-239.e6.